Genotypic and phenotypic diversity within the neonatal HSV-2 population

Lisa N. Akhtar[1,5], Christopher D. Bowen[2], Daniel W. Renner[2], Utsav Pandey[2], Ashley N. Della Fera[3], David W. Kimberlin[4], Mark N. Prichard[4], Richard J. Whitley[4], Matthew D. Weitzman[3,5]*, Moriah L. Szpara[2]*

[1] Department of Pediatrics, Division of Infectious Diseases, Children's Hospital of Philadelphia

[2] Department of Biochemistry and Molecular Biology, Center for Infectious Disease Dynamics, and the Huck Institutes of the Life Sciences, Pennsylvania State University

[3] Department of Pathology and Laboratory Medicine, Division of Protective Immunity and Division of Cancer Pathobiology, Children's Hospital of Philadelphia

[4] Department of Pediatrics, Division of Infectious Diseases, University of Alabama at Birmingham

[5] University of Pennsylvania Perelman School of Medicine

***Corresponding Authors**
Moriah L. Szpara
Dept. of Biochemistry & Molecular Biology
The Huck Institutes of the Life Sciences
W-208 Millennium Science Complex (MSC)
Pennsylvania State University
University Park, PA 16802 USA
Phone: 814-867-0008
orcid.org/0000-0001-9859-1678
Email: moriah@psu.edu

Matthew D. Weitzman
Division of Protective Immunity
The Children's Hospital of Philadelphia
4050 Colket Translational Research Building
3501 Civic Center Blvd
Philadelphia, PA 19104-4318
Phone: 267-425-2068
orcid.org/0000-0001-9713-167X
Email: weitzmanm@email.chop.edu

Author emails:
Lisa N. Akhtar: AkhtarL@email.chop.edu
Christopher D. Bowen: cdb5004@psu.edu
Daniel W. Renner: dwr19@psu.edu
Utsav Pandey: uup104@psu.edu
Ashley N. Della Fera: ashleyycoxx@gmail.com
David W. Kimberlin: DKimberlin@peds.uab.edu
Mark N. Prichard: MPrichard@peds.uab.edu
Richard J. Whitley: RWhitley@peds.uab.edu
Matthew D. Weitzman: weitzmanm@email.chop.edu
Moriah L. Szpara: moriah@psu.edu

Keywords: Neonatal, herpes simplex virus 2, human herpesvirus 2, comparative genomics, viral spread, minority variants

18 # Abstract

19 More than 14,000 neonates are infected with herpes simplex virus (HSV) annually.
20 Approximately half display manifestations limited to the skin, eyes, or mouth (SEM disease).
21 The rest develop invasive infections that spread to the central nervous system (CNS disease or
22 encephalitis) or systemically (disseminated disease). Invasive HSV disease is associated with
23 significant morbidity and mortality, but viral and host factors that predispose neonates to these
24 forms are unknown. To define viral diversity within the infected neonatal population, we
25 evaluated ten HSV-2 isolates from newborns with a range of clinical presentations. To assess
26 viral fitness independent of host immune factors, we measured viral growth characteristics in
27 cultured cells and found diverse *in vitro* phenotypes. Isolates from neonates with CNS disease
28 were associated with larger plaque size and enhanced spread, with isolates from cerebrospinal
29 fluid (CSF) exhibiting the most robust growth. We sequenced complete viral genomes of all ten
30 neonatal viruses, providing new insights into HSV-2 genomic diversity in this clinical setting.
31 We found extensive inter-host and intra-host genomic diversity throughout the viral genome,
32 including amino acid differences in more than 90% of the viral proteome. The genes encoding
33 glycoprotein G (gG, US4), gI (US7), gK (UL53), and viral proteins UL8, UL20, UL24, and US2
34 contained variants that were found in association with CNS isolates. Many of these viral proteins
35 are known to contribute to cell spread and neurovirulence in mouse models of CNS disease. This
36 study represents the first application of comparative pathogen genomics to neonatal HSV
37 disease.

38

39 # Importance

40 Herpes simplex virus (HSV) causes invasive disease in half of infected neonates, resulting in
41 significant mortality and permanent cognitive morbidity. The factors that contribute to invasive
42 disease are not understood. This study reveals diversity among HSV isolates from infected
43 neonates, and makes the first associations between viral genetic variations and clinical disease
44 manifestations. We found that viruses isolated from newborns with encephalitis show enhanced
45 spread in culture. These viruses contain protein-coding variations not found in viruses causing
46 non-invasive disease. Many of these variations are found in proteins known to impact
47 neurovirulence and viral spread between cells. This work advances our understanding of HSV
48 diversity in the neonatal population and how it may impact disease outcome.

49

50 # Introduction

51 Each year an estimated 10,000 neonates are infected with HSV-2, and 4,000 infected with HSV-
52 1, worldwide (1). Infants are typically infected at the time of birth by maternal genital shedding
53 of HSV, most often by mothers who are not aware of their infection (2–4). The recent increase in
54 genital HSV-1 incidence among women of childbearing age, particularly in developed nations,
55 suggests that the burden of neonatal infection will continue to rise (1, 5). While some infected
56 infants exhibit only superficial infection limited to the skin, eyes, or mouth (SEM disease; 45%),
57 about half develop invasive systemic (disseminated disease; 25%) or central nervous system
58 (CNS disease; 30%) infections associated with significant morbidity and mortality (6, 7).
59 Currently, the antiviral medication acyclovir is the standard therapy for all forms of neonatal

60 HSV disease. Although this intervention has reduced mortality due to invasive disease, most
61 survivors of invasive disease are left with permanent neurodevelopmental deficits (8, 9).

62 The factors that predispose a neonate to invasive HSV infection are not entirely known. Recent
63 studies have found that some adults and children outside of the neonatal period who experience
64 HSV infection of the brain have a host genetic defect within the Toll-like receptor-3 (TLR3)
65 pathway (10, 11). Outside of the neonatal period, HSV encephalitis is rare, as are host defects in
66 the TLR3-pathway. By contrast, half of HSV-infected neonates experience invasive CNS or
67 disseminated disease, making it less likely that host genetic defects alone could account for all of
68 the observed cases of invasive infection in neonates. Prior clinical data on mother-to-infant
69 transmission of HSV indicate that most cases of neonatal disease, including invasive forms of
70 disease, result from newly acquired or primary HSV infection prior to the development of
71 maternal antibody production (2–4, 12). This suggests a window of opportunity where the
72 contributions of viral genetic variation to the progression of invasive infection and disease may
73 be greater than in adults.

74 Prior studies have identified viral genetic factors that influence virulence or disease for
75 reoviruses, influenza virus, HIV, and others (13–18). In contrast to these RNA viruses, HSV was
76 presumed to have lower genetic diversity and potential for variation in virulence, due to its
77 relatively stable DNA genome and long co-evolutionary history with humans (19). The
78 assumption of limited HSV heterogeneity was supported by early studies that utilized low-
79 resolution restriction fragment length polymorphism (RFLP) or single-gene analyses to compare
80 multiple HSV isolates (20–22). However Rosenthal and colleagues used RFLP and PCR analysis
81 of a single locus to demonstrate that a heterogeneous HSV population can exist in an invasive

82 neonatal infection, and provided proof of principle that natural genetic variation can impact
83 neurovirulence (23, 24). More recently, advances in high-throughput sequencing (HTSeq) have
84 enabled a re-evaluation of herpesvirus genome-wide variation, which suggests that herpesviruses
85 harbor extensive diversity both between strains or individuals (inter-host variation) as well as
86 within a single individual (intra-host variation) (25–27). These minor genetic variants may
87 become clinically important if a variant within the viral population becomes the new dominant
88 allele or genotype as a result of a bottleneck at transmission, entry into a new body compartment,
89 or selective pressure such as antiviral therapy (28, 29).

90 Several recent examples have demonstrated the potential for new insights gained by applying
91 HTSeq approaches to herpesvirus infections in a clinical setting. In HTSeq studies of congenital
92 infection by the beta-herpesvirus human cytomegalovirus (HCMV), Renzette *et al.* found
93 evidence for heterogeneous viral populations both within and between hosts (30–35). The levels
94 of diversity observed in congenital HCMV infections far exceeded those observed in adult
95 infections (36–38). HTSeq-based examination of vaccine-associated rashes due to the alpha-
96 herpesvirus varicella zoster virus (VZV) demonstrated that adult skin vesicles contain a subset of
97 the viral population introduced during vaccination, and found at least 11 VZV genomic loci that
98 were linked to rash formation (26). Recent HTSeq comparisons of adult genital HSV-2 revealed
99 the first evidence of a single individual shedding two distinct strains (39), demonstrated changes
100 in the viral genome over time in a recently infected host (40), and provided the first evidence of
101 ancient recombination between HSV-1 and HSV-2 (41, 42). However, to date there has been no
102 evaluation of genome-wide variation in neonatal HSV isolates to determine the levels of
103 diversity in this population, or the potential impact(s) of viral genetic variants on disease.

104 Until recently, several technical barriers prevented thorough assessment of neonatal HSV
105 genomes. A key constraint on studies of neonatal disease has been the availability of cultured,
106 minimally-passaged viral samples that are both associated with clinical information and have
107 also been maintained in a low-passage state that is appropriate for sequencing and further
108 experimental studies. Historically viral culture was part of the HSV diagnostic workflow, but this
109 has been superseded in clinical laboratory settings by the speed and sensitivity of viral detection
110 by PCR (43, 44, 6). This change limits neonatal HSV sample availability for *in vitro* and animal
111 model studies. In addition, many previously archived neonatal HSV isolates have been passaged
112 extensively, allowing them to acquire mutations that enhance viral growth in culture (23, 24).
113 Additional challenges for HTSeq approaches to neonatal HSV include the large size of the viral
114 genome (~152 kb), its high G+C content (~70%), and a large number of variable-number tandem
115 repeats in the viral genome (> 240 mini/micro-satellite repeats and >660 homopolymers of ≥6
116 base pairs) (45, 27). Therefore, many studies of HSV diversity (21, 46–49) or the effect of HSV
117 genetic variation on disease (50–52) have relied on low-resolution restriction fragment length
118 polymorphism (RFLP) or single-gene PCR analyses, due to the speed and ease of analysis in
119 comparison to whole-genome approaches (53–58). To overcome these challenges, we combined
120 our expertise in HSV comparative genomics and phenotypic analysis (59, 53, 60, 58) with a
121 unique resource of low-passage, well-annotated neonatal specimens (8, 61, 9).

122 Here we analyzed a set of ten low-passage clinical HSV-2 isolates collected from neonates with
123 HSV infection, enrolled in one of two clinical studies that spanned three decades of patient
124 enrollment (1981-2008) (8, 61, 9). These samples represented a wide range of clinical
125 manifestations including SEM, CNS, and disseminated disease, and each sample was associated
126 with de-identified clinical information. We defined the level of diversity in this population using

127 comparative genomics and an array of cell-based phenotypic assays. We found that HSV-2
128 isolates displayed diverse *in vitro* phenotypes, as well as extensive inter- and intra-host diversity
129 distributed throughout the HSV-2 genome. Finally, we found coding variations in several HSV-2
130 proteins associated with CNS disease. This study represents the first-ever application of
131 comparative pathogen genomics to neonatal HSV disease and provides a basis for further
132 exploration of genotype-phenotype links in this clinically vulnerable patient population.

133 Results

134 Neonatal HSV-2 samples represent a diverse clinical population

135 We utilized samples collected from ten HSV-2-infected neonates enrolled by the National
136 Institute of Allergy and Infectious Diseases Collaborative Antiviral Study Group (CASG) for
137 clinical trials between 1981 and 2008 (8, 61, 9). These infants encompassed a range of clinical
138 disease manifestations (see **Table 1**), with about half experiencing invasive CNS disease (5
139 patients) or disseminated (DISS) disease with CNS involvement (2 patients), and the remainder
140 experiencing non-invasive SEM disease (3 patients). Extensive clinical information was
141 available for each patient, including long-term neurocognitive and motor outcomes (**Table 1**).
142 This population was also diverse with respect to sex, race, gestational age, and enrollment center
143 (**Table 1**; enrollment center data not shown). All samples were collected at the time of diagnosis,
144 prior to initiation of acyclovir therapy. Each isolate was cultured once as part of the diagnostic
145 process, with expansion only for the experiments shown here. Although the sample size was
146 constrained by the rarity of neonatal HSV infection and availability of appropriately maintained
147 isolates, our group is similar in size to prior HTSeq comparisons of congenital HCMV samples

148 (31, 32, 34, 35), and is the largest group of neonatal HSV samples ever subjected to comparative
149 genomic and phenotypic analysis.

150 Neonatal HSV-2 isolates have different fitness in culture

151 To determine whether the viruses isolated from this neonatal population **(Table 1)** were
152 intrinsically different, we assessed viral growth in culture, which provides a consistent
153 environment that is independent of host genetic variation. To minimize the impact of immune
154 pressure we selected Vero monkey kidney cells, which lack an interferon response (62, 63). Each
155 viral isolate was applied to a confluent monolayer of cells *in vitro*, and allowed to form plaques
156 for 100 hours (h) (**Figure 1A**). Average plaque size differed between isolates, with six of the ten
157 isolates being statistically larger (indicated in green) than the other four (indicated in black,
158 **Figure 1B**) (one-way ANOVA with Holm-Sidak's multiple comparisons test, $p<0.05$). The
159 average plaque size of the previously described low passage, adult HSV-2 isolate SD90e is
160 shown for comparison (64). The largest plaque sizes were observed in the two viruses isolated
161 directly from the cerebrospinal fluid (CSF; isolates CNS11 and DISS14; **Figure 1B**); these two
162 isolates were not statistically different from one another in size, but were significantly larger than
163 any of those isolated from the skin (one-way ANOVA with Holm-Sidak's multiple comparisons
164 test, $p<0.05$). Plaque size was assessed at each passage in culture and remained constant from the
165 time the isolates were received in our laboratory (passage 2) through their genetic and
166 phenotypic analysis (passage 4). The variance in plaque sizes produced by a given isolate was
167 not statistically different between isolates **(Figure 1B)**. The differences in average plaque size
168 between isolates suggested that the HSV-2 populations found in each neonatal isolate are indeed
169 intrinsically different.

170 **Entry kinetics, DNA replication, protein expression, and virus production do not**
171 **account for differences in plaque size**

172 Plaque formation is a complex endpoint that involves the ability of the virus to enter the cell,
173 replicate its double stranded DNA genome, produce viral proteins and assemble new virions that
174 spread to adjacent cells. Therefore, we explored whether the differences in plaque formation
175 observed in Vero cells reflected inherent differences in the ability of isolates to complete each of
176 these stages of the viral life cycle. For these comparisons, two large-plaque-forming isolates
177 (CNS11 and CNS03) were compared to two small-plaque-forming isolates (CNS12 and SEM02).
178 First, we compared each isolate's rate of cell entry. Virus was applied to chilled cells, followed
179 by warming to synchronize cell entry **(Figure 2A).** A low pH solution was applied at various
180 points over the first hour of cell entry to inactivate any virus that had not yet entered a cell, and
181 plaque formation was then allowed to proceed for 100 h. We found no difference in rates of cell
182 entry between these four representative viral isolates (**Figure 2B**), suggesting that large plaques
183 did not result from increased rates of virus entry into cells.

184 We next infected Vero cells at high multiplicity of infection (MOI=5) to compare the outcome of
185 a single round of viral replication. We found that all four isolates produced similar numbers of
186 genome copies (as measured by qPCR for the gB gene; see Methods for details) **(Figure 2C**),
187 indicating that differences in viral DNA replication did not influence plaque size. We quantified
188 the production of infectious virus by counting plaque-forming-units (PFU) on Vero cell
189 monolayers, as well as on the highly-permissive U2OS human bone osteosarcoma epithelial cell
190 line (65). No differences in virus production were noted between the four isolates when
191 quantified on either cell type (**Figure 2D, 2˜E**). U2OS cells lack innate sensing of viral infection

192 through the STING pathway (66) and can even support the growth of highly-defective HSV-
193 isolates that lack ICP0 function (65). All isolates formed large plaques on the highly-permissive
194 U2OS cell monolayers (**Figure S1**), allowing us to rule out the possibility that very small foci of
195 infection were missed during titering of the small plaque-forming isolates on Vero cells (**Figure**
196 **2D, E**). Finally, we compared viral protein production for these isolates, and found no
197 differences in the expression levels of a panel of HSV-2 viral proteins at either early (6 h post
198 infection, hpi) or late (24 hpi) time points of a single round of high MOI infection (**Figure 2F,**
199 **G**; see legend for list of proteins). Taken together, these results suggested that large- and small-
200 plaque-forming neonatal HSV-2 isolates did not differ significantly in viral entry, DNA
201 replication, infectious virus production, or protein production over a single round of infection.

202 Large-plaque-forming isolates exhibit enhanced cell-to-cell spread

203 We next assessed the ability of representative large- and small-plaque-forming isolates to spread
204 from cell-to-cell. Vero cell monolayers were infected at low MOI (MOI=0.001) in order to assess
205 differences over multiple rounds of viral replication and spread throughout the cell monolayer
206 (**Figure 3A**). The contribution of indirect cell-free spread was minimized by including 0.1%
207 human serum in the media, and changing the media every 24 h to remove released virus and
208 refresh serum levels. Over a 72-hour time course, cell monolayers were assessed to measure the
209 extent of cell-to-cell spread, either by harvesting and titering PFU production (**Figure 3B-C**), or
210 by fixing infected cell monolayers and evaluating the distribution of virus by
211 immunofluorescence (**Figure 3D**, **E**, and **Figure S2**). Viral titers recovered from harvested cells
212 were similar at 2 hpi, confirming that equivalent amounts of each virus were present following
213 initial infection (**Figure 3B**). By 72 hpi, after multiple rounds of replication and spread, the

214 large-plaque-forming isolates CNS11 and CNS03 had achieved viral titers significantly greater
215 than those of the small-plaque-forming isolates CNS12 and SEM02 (**Figure 3B, C**; two-way
216 ANOVA followed by Tukey's multiple comparison test, $p<0.0001$ at 72h). Isolate CNS11,
217 which was obtained directly from the CSF, produced titers statistically greater than the other
218 three isolates **(Figure 3B, C)**.

219 We also directly evaluated cell-to-cell spread by immunostaining and quantifying the distribution
220 of infected cells around each infectious focus. Infected Vero cell monolayers were fixed at 24,
221 48, and 72 hpi, and subjected to fluorescent immunocytochemistry with an antibody directed
222 against total HSV (**Figure 3D** and **Figure S2**). The region of HSV-positive cells surrounding a
223 single initial infection was greater for the large-plaque-forming neonatal HSV-2 isolates at 24
224 hpi, and increased by 48 and 72 hpi. The central cytolytic clearings seen in the monolayers
225 infected by CNS11 or CNS03 were approximately two-fold greater than those infected by
226 CNS12 or SEM02, reflecting the average two-fold increase in plaque size observed in
227 methylene-blue-stained monolayers in **Figure 1**. However, the region of infected cells
228 surrounding the central cytolytic clearing for CNS11 and CNS03 was dramatically larger than
229 for CNS12 and SEM02, suggesting that large-plaque-forming neonatal HSV-2 isolates show
230 greater spread from cell-to-cell than could have been predicted by measuring plaque size alone.
231 To quantify this increase in the area of infected cells after a low-MOI infection, each coverslip
232 was imaged **(Figure S2)** and the total number of immunofluorescent pixels was quantified
233 (**Figure 3E**). By 72 hpi, the area of HSV-infected cells was statistically greater for the large-
234 plaque-forming isolates CNS11 and CNS03, as compared to the small-plaque-forming isolates
235 CNS12 and SEM02 (two-way ANOVA followed by Tukey's multiple comparison test, $p<0.05$ at
236 72h). Together these data indicated that large-plaque-forming isolates shared an enhanced ability

237 to spread cell-to-cell through culture, in comparison to small-plaque-forming isolates.

238 Comparative genomics reveals genetic diversity in neonatal HSV-2 isolates

239 The differences identified in cell-to-cell spread between neonatal isolates in culture indicated the
240 existence of intrinsic differences between these viruses. To reveal how genetic variation may
241 contribute to viral phenotypes in culture, and ultimately to clinical disease manifestations, we
242 sequenced the complete viral genome of all ten neonatal HSV-2 isolates. For each isolate, we
243 sequenced purified viral nucleocapsid DNA and assembled a consensus genome, which
244 represents the most common genotype at each nucleotide locus in the viral population. The
245 clinical trials utilized in this study enrolled HSV-infected infants from multiple sites across the
246 United States (8, 9, 61). Therefore, we first assessed the overall degree of relatedness between
247 these viral genomes to understand whether any similarities in viral or geographic origin might
248 have contributed to *in vitro* or clinical phenotype patterns. In light of the known potential for
249 recombination in the phylogenetic history of HSV (49, 67, 53, 42), we used a graph-based
250 network to investigate the phylogenetic relationship between these isolates. We found a similar
251 degree of divergence among all ten neonatal HSV-2 consensus genomes (**Figure 4A**). We then
252 compared these ten neonatal HSV-2 genomes to all available HSV-2 genomes in GenBank (all of
253 which are adult; see **Table S1** for HSV-2 GenBank accessions and references) to discern any
254 geographic or other clustering (see **Table 1**). The neonatal isolates did not segregate into any
255 exclusive groupings, but instead intermingled among non-neonatal isolates, with deep branches
256 between each isolate (**Figure 4B**). These findings were corroborated using an alternative
257 phylogenetic clustering algorithm as well (**Figure S3**). This suggested that similarities in viral
258 genetic origin were not responsible for determining the cellular or clinical outcomes of neonatal

259 HSV-2 infection.

260 Overall protein-coding diversity in neonatal HSV-2 isolates is similar to that 261 observed in adult HSV-2 strains

262 We next asked whether overt defects in any single HSV-2 protein might be associated with
263 clinical or *in vitro* spread phenotypes. In examining the coding potential of all ten neonatal HSV-
264 2 isolates, we found no protein deletions or truncations encoded by any of these viral genomes.
265 These comparisons revealed a total of 784 nucleotide differences in 71 genes (see **Table S2**),
266 resulting in 342 non-synonymous AA differences in 65 proteins. This led to an average of 1%
267 coding variation (range 0.0 : 2.6%). This variation was spread widely throughout the HSV-2
268 genome, without concentration in a particular genomic region or category of protein function
269 **(Figure 5).** We found a similar level of coding diversity in this set of neonatal isolates as in a
270 comparable set of 10 adult HSV-2 isolates **(Figure 5, Table S2).** We also compared these
271 neonatal genomes to the full set of 58 annotated adult HSV-2 genomes from GenBank (listed
272 **Table S1**). As expected from the difference in sample size, there was more overall diversity
273 found across 58 adult HSV-2 genomes than in 10 neonatal genomes. A comparison of the dN/dS
274 ratio in neonatal vs. adult HSV-2 genomes revealed a similar trend with a few outliers visible on
275 each axis, e.g. UL38 and US8A had a higher dN/dS ratio in neonatal than in adult isolates (see
276 **Table S2** and **Figure S4** for full comparison). These data indicated that at the consensus level,
277 neonatal HSV-2 isolates display substantial inter-host coding diversity spread throughout the
278 genome, but do not possess strikingly more diversity or an excess of genetic drift as compared to
279 adult isolates.

280 **Minority variants expand the potential coding diversity of neonatal HSV-2 isolates**

281 We next focused our attention on differences below the consensus level in each intra-host viral
282 population. The amino acid (AA) variations described above exist in the consensus genomes of
283 each isolate. Since viral replication creates a population of genomes, we next assessed whether
284 minor allelic variants existed within the viral population of any neonatal HSV-2 isolate, thereby
285 expanding the viral genetic diversity within each host. The significant depth of coverage from
286 deep-sequencing of each isolate allowed us to search for minority variants at every nucleotide
287 position of each genome. We defined a minor variant as any nucleotide allele (single nucleotide
288 polymorphism, or SNP) or insertion/deletion (INDEL) with frequency below 50%, but above 2%
289 (a conservative limit of detection; see Methods for additional criteria). We found minor variants
290 in the viral genome population of all 10 neonatal HSV-2 isolates, albeit to a different degree in
291 each isolate (**Figure 6A** and **Table S3).** In total, there were 1,821 minor variants, distributed
292 across all genomic regions (**Figure S5; Table S3**). For both SNPs and INDELs, intergenic
293 minority variants outnumbered those in genes (genic), likely reflecting the higher selective
294 pressures against unfavorable mutations in coding regions. The neonatal isolate DISS29 had 8-
295 10-fold higher levels of minority variants than other neonatal isolates (**Figures 6A and S5**), and
296 these variants were often present at a higher frequency or penetrance of the minor allele than
297 observed in other neonatal isolates (**Figures 6B and S5).** We further examined the distribution of
298 minor variants that occurred in genes, and found that nearly every HSV-2 protein harbored
299 minority variants in at least one neonatal isolate (**Figure 6C**). Only UL3, UL11, UL35, and
300 UL55 were completely devoid of minority variants. Three of these genes (UL3, UL11, UL35)
301 were also devoid of AA variations at the consensus level (**Figure 5).** These data revealed the
302 breadth of potential contributions of minority variants to neonatal HSV-2 biology, which could

303 undergo selection over time or in specific niches.

304 **Coding variations identified in neonatal HSV-2 isolates associated with CNS disease**

305 To understand how viral genetic variants might relate to clinical disease, we assessed whether
306 any of the consensus level coding variations identified in our group of ten neonatal HSV samples
307 segregated with clinical disease features. A number of AA variations were shared by the CSF-
308 derived isolates CNS11 and DISS14, which formed the largest plaques *in vitro*. These included
309 AA variants at the level of the consensus genome in the HSV-2 genes encoding glycoprotein K
310 (gK, UL53 gene: V323M), glycoprotein I (gI, US7 gene: R159L and P215S), UL8 (R221S), US2
311 (F137L), and glycoprotein G (gG, US4 gene: R338L, S442P, and E574D) (**Figure 7**). The gI
312 variants exist individually in other viral isolates obtained from neonates with CNS disease
313 (**Table S4**). Isolates collected from infants experiencing disseminated disease with CNS
314 involvement also shared a variant in the HSV-2 UL20 gene (P129L) (**Figure 7**). One variant in
315 the HSV-2 UL24 gene (V93A) was shared only by isolates from infants with SEM disease, with
316 all isolates from infants with CNS disease containing a valine at this position **(Figure 7).** The
317 sample size of these comparisons was constrained by the overall limits of neonatal HSV-2 isolate
318 availability. While CNS11 and DISS14 shared several variants listed in **Figure 7**, these viral
319 genomes were not similar at the consensus genome level (**Figure 4**). These isolates also had non-
320 shared coding differences in the same genes that contained shared variants (e.g. gK, UL8, gG).
321 This indicates a potential for convergent evolution at these loci. Many of the coding variations
322 identified in this dataset involve viral proteins that are known to modulate cell-to-cell spread
323 (68–72) and/or contribute to neurovirulence in mouse models of CNS infection (70, 73–79)
324 (**Figure 7** and **Table S4**), however, their role in human disease has not yet been assessed.

325 # Discussion

326 Host factors have not been identified to explain the >50% of neonates experiencing invasive
327 CNS or disseminated forms of HSV infection. There is growing evidence that most
328 herpesviruses, including HSV-1 and HSV-2, contain significant genetic variation (53, 27, 56,
329 80–82). The potential contributions of viral genetic variation to clinical disease in neonates
330 therefore warrants exploration. Here, we analyzed genetic and phenotypic diversity for HSV-2
331 isolated from ten neonatal patients spanning two clinical studies (8, 61, 9). Although this group is
332 small, the associations identified here provide the first insights into the potential impact of viral
333 variability on clinical outcomes in neonatal HSV disease, and serve as a starting point for further
334 mechanistic investigation. We found that these ten neonatal HSV-2 isolates exhibited diverse
335 growth characteristics in culture, with larger plaque-forming isolates observed more often in
336 infants with CNS as opposed to SEM disease. Furthermore, we established that enhanced viral
337 spread through culture was the main contributor to this large plaque formation. Using
338 comprehensive comparative genomics, we further demonstrated that these neonatal HSV-2
339 isolates contained extensive genetic diversity both within and between hosts. These data revealed
340 several specific viral genetic variations that were associated with cases of CNS disease, in
341 proteins known to contribute to cell-to-cell spread and/or neurovirulence in mouse models of
342 CNS disease. Further studies are required to determine the impact of these variations on HSV-2
343 neurovirulence and progression to CNS disease.

344 Genomic comparison of these neonatal isolates revealed a wide range of genetic diversity. At the
345 consensus genome level, which reflects the most common allele in each viral population, we
346 found that coding differences between strains were as numerous as between previously described

347 sets of adult HSV-2 isolates **(Figure 5)** (80–82). Furthermore, the specific genetic variations
348 associated with neonatal CNS disease in our study can also be found in genital HSV-2 isolates
349 which are not associated with CNS disease in adults. This suggests that the dramatic differences
350 in clinical manifestations following HSV-2 infection in neonates, with significantly higher rates
351 of invasive CNS infection, are not due to unique neonatal HSV-2 strains. It is more likely that
352 genetic variations occurring naturally in the adult HSV-2 population, when present in the specific
353 context of neonatal infection, may confer neurovirulence and progression to CNS disease.

354 At the level of minority variants (MV), which represent rare alleles that exist within each intra-
355 host viral population, we found that the DISS29 harbored 8-10 fold and CNS15 harbored 3-4
356 fold more MV than other neonatal virus genomes (**Figures 6 and S4**). This could be indicative
357 of a mixed viral population (e.g. a multi-strain infection) or of decreased polymerase fidelity (28,
358 27). Diversity in viral populations has also been observed in congenital HCMV infection (31, 32,
359 35, 34). However, this is the first time that evidence has been found for this level of viral
360 population diversity with HSV-2. These minor genotypes may be selected or genetically isolated
361 in particular niches (e.g. CSF), as observed in a comparison of VZV skin vesicles (26), or by
362 antiviral drug selection, as was recently demonstrated in two adults with genital HSV-2 infection
363 (83). All of the isolates sequenced in this study were collected at the initial time of diagnosis
364 (≤19 days old), prior to acyclovir treatment and prior to the development of an HSV-specific
365 immune response. It would therefore be compelling to examine the viral genome population
366 from serial patient isolates over time to identify shifts in the frequency of MV due to antiviral or
367 immune selection. Isolates from different body sites of the same patient could likewise be
368 compared to determine whether particular genotypes are enriched in different body niches.

369 This comparison of viral genotype to clinical phenotype revealed associations between neonatal
370 CNS disease and several viral protein variants that may impact neurovirulence through
371 modulation of cell-to-cell spread. Although the sample set in this proof of concept study is small,
372 we observed potential patterns that warrant exploration in a larger dataset. It is important to
373 acknowledge that there is limited availability of samples from neonatal infection, both due to the
374 rarity of these infections, and the fragility and limited body size of the infected infants. These
375 natural circumstances lead to minimal sample collection from infected neonates. The finding that
376 CNS-associated isolates in our study often exhibit enhanced spread between cells in culture,
377 particularly those derived directly from the CSF, suggests that one or more of these variants
378 could be functionally significant. Coding differences in viral proteins not known to contribute to
379 neurovirulence were also found to be associated with neonatal CNS disease, and represent
380 potential novel contributions to invasive infection. These promising results warrant exploration
381 in a larger study, ideally with isolates from multiple time points and/or body sites from each
382 infected infant. This would enable a better understanding of how overall viral genetic diversity
383 contributes to neuroinvasion.

384 # Methods

385 ## Viruses

386 Viruses were collected from neonates enrolled in clinical studies (8, 9, 61) by the Collaborative
387 Antiviral Study Group (CASG) at the University of Alabama Birmingham (UAB). Samples were
388 collected from either the cerebrospinal fluid (CSF) or skin. Enrollment in original studies was
389 evenly split between males and females, and included both black and white patients. Clinical

390 morbidity score was determined at 12 months of life as previously defined (84, 12). Initial
391 collection of samples, use of samples in this study, and use of de-identified clinical information
392 was approved by the UAB Institutional Review Board. See Supporting Information for
393 additional details of this and subsequent methods.

394 **Cell culture**

395 Human lung fibroblast MRC-5 cells (ATCC®, CCL-171), African green monkey kidney Vero
396 cells (ATCC®, CCL-81), and human epithelial bone osteosarcoma U2OS cells (ATCC®, HTB-
397 96) were cultured under standard conditions. Cell lines were authenticated by ATCC prior to
398 purchase, and were confirmed to be mycoplasma free throughout experiments by periodic testing
399 (LookOut Mycoplasma, Sigma).

400 **Virus culture**

401 Viruses were cultured at the time of diagnosis and snap frozen after 1 passage. Each viral isolate
402 was then passaged 3 times on MRC-5 cells at a MOI of 0.01, with harvest at the time of
403 complete cytopathic effect (between 50-70 h). Viral stocks were titered on either Vero cells (100
404 h) or U2OS cells (48 h) under a methylcellulose overlay. Plaque size and morphology did not
405 change for any viral isolates over the course of virus stock expansion.

406 **Plaque measurements**

407 Plaques were stained with 0.5% methylene blue. Serial 4X brightfield images were collected on
408 an EVOS FL Auto Imaging System and stitched by EVOS software (University of Pennsylvania
409 Cell and Developmental Biology Microscopy Core). Plaque area was measured using ImageJ

410 software.

411 Genome copy number estimation by quantitative PCR for UL27

412 DNA was extracted and quantitative PCR was performed with primers specific to the viral
413 glycoprotein B gene (gB; UL27) (43). Absolute quantification was calculated based on a
414 standard curve of HSV-1 strain F nucleocapsid DNA (59).

415 Viral entry assay

416 Monolayers of Vero cells were cooled to 4°C for 30 minutes prior to infection with 100 PFU of
417 each viral isolate. After 1 h of viral incubation at 4°C, unbound virus was removed by washing
418 and cells were moved to 37°C. At 0, 10, 20, 30, 45, or 60 minutes, a low-pH citrate buffer was
419 applied to inactivate extracellular virus. For each condition, parallel infections were performed
420 without the addition of citrate solution (control). Cell monolayers were washed and allowed to
421 form plaques under methylcellulose for 100 h. Viral entry was quantified as the fraction of
422 plaques formed following citrate buffer application, where 100% is the number of plaques
423 formed on a monolayer not treated with citrate buffer (control).

424 Single-step and multi-step growth curves

425 Growth curves of HSV infection were performed in Vero cells. At 2 hpi, 0.1% human serum was
426 added to reduce cell-free spread of virus. Single-step growth curves were performed at MOI=5,
427 and multi-step growth curves at MOI=0.001, as defined by titering viral stocks on U2OS cells.
428 Every 24 h, the supernatant was removed and media containing 0.1% human serum reapplied.

429 **Immunocytochemistry**

430 Immunocytochemistry was performed as previously described (85). Infection was detected with
431 rabbit anti-HSV primary antibodies (Agilent Dako, B0114) and fluorophore-conjugated anti-
432 rabbit secondary antibodies (Invitrogen, A-11008). Cell nuclei were counterstained with DAPI.
433 5X images were collected with a Leica DM6000 wide field microscope equipped with a
434 Photometrics HQ2 high resolution monochrome CCD camera, and processed with LAS AF
435 software (UPenn Cell and Developmental Microscopy Core). 10X images were collected on an
436 EVOS FL Auto Imaging System and stitched using EVOS software (UPenn Cell and
437 Developmental Microscopy Core). Exposure and gain were optimized within each experiment
438 for one virus at the 72 h time point and applied identically to each image within that experiment.
439 Subsequent image processing (ImageJ) was applied equally to all images in a given experiment.

440 **Immunoblotting**

441 Immunoblotting was performed as previously described (85). Equal amounts of whole cell lysate
442 were separated by SDS-PAGE. Membranes were immunoblotted with antibodies raised against
443 total HSV (Agilent Dako, B0114); glycoproteins (g)C, gD, gE, gH, and VP5 (all gifts from Gary
444 Cohen); ICP8 (gift from David Knipe); and GAPDH (GeneTex, GTX100118).

445 **Viral DNA isolation and Illumina sequencing**

446 Viral nucleocapsid DNA for genome sequencing was prepared by infecting MRC-5 cells at an
447 MOI ≥5 as previously described (86, 87). Viral nucleocapsid gDNA was sheared using a Covaris
448 M220 sonicator/disruptor under the following conditions: 60s duration, peak power 50, 10% duty
449 cycle, at 4°C. Barcoded sequencing libraries were prepared using the Illumina TruSeq low-

450 throughput protocol according to manufacturer's specifications and as previously described (60,
451 88). The quality of sequencing libraries was evaluated by Qubit (Invitrogen, CA), Bioanalyzer
452 (Agilent), and qPCR (KAPA Biosystems). Paired-end sequencing (2 × 300bp length) was
453 performed on an Illumina MiSeq, according to manufacturer's recommendations (17pM input).

454 ***De novo* genome assembly**

455 A consensus genome was assembled for each viral isolate using a previously described Viral
456 Genome Assembly (VirGA) bioinformatics workflow (60). Annotation of new genome
457 sequences was guided by the HSV-2 reference genome (strain HG52; GenBank NC_001798)
458 based on sequence homology (89).

459 **Comparative genomics and phylogenetic analysis**

460 The 10 neonatal HSV-2 genomes were aligned with all annotated HSV-2 genomes available in
461 GenBank (see **Table S1** for full list of 58 genomes; all derived from adults) using MAFFT (90).
462 The genome-wide alignment used a trimmed genome format (lacking the terminal repeats) to
463 avoid giving undue weight to these duplicated sequences. The MAFFT alignment was used to
464 generate a NeighborNet phylogenetic network in SplitsTree with Uncorrected P distances (49,
465 91, 92), as well as a Neighbor-Joining tree (Jukes-Cantor, 1000 bootstraps) in MEGA Omega for
466 Windows (93). A diverse subset of ten adult HSV-2 isolates was selected for protein-level
467 comparisons with the ten neonatal isolates (indicated in **Table S1** with an asterisk). ClustalW2
468 was used to construct pairwise nucleotide alignments between whole genomes, and pairwise
469 amino acid alignments for each gene and protein (94). Pan-HSV2 comparisons excluded three
470 viral proteins for which sequences are not fully determined in most published strains, likely due

471 to the high G+C-content and numerous tandem repeats in these regions: ICP34.5 (RL1 –
472 annotated/complete in only 9 genomes from **Table S1**), ICP0 (RL2 – annotated/complete in only
473 8 genomes from **Table S1**), and ICP4 (RS1 – annotated/complete in only 6 genomes from **Table**
474 **S1**) (80–82). Custom Python scripts were used on these alignments to identify nucleotide and
475 AA differences between samples.

476 **Minority variant detection & quantification**

477 Minority variants (MV) were detected using VarScan v2.2.11 (mpileup2snp and mpileup2indel
478 commands) (95), using the following parameters to differentiate true MV from technical artifacts
479 (26): minimum allele frequency ≥ 0.02 (2%); base call quality ≥ 20; read depth ≥ 100;
480 independent reads supporting minor allele ≥5. MV with directional strand bias ≥ 90% were
481 excluded. The genomic location and potential impact of each MV was assessed using SnpEff and
482 SnpSift (96, 97). We use the conservative cutoff of 2% for detection of minority variants both to
483 avoid false positive signals and to provide data that is comparable to recent examples in the
484 genomic analysis of herpesviruses in clinical samples (98, 28, 99).

485

486 **Acknowledgements**

487 We thank Penny Jester and the UAB clinical support team for their assistance in retrieving
488 archival records. The UPenn Cell and Developmental Biology Microscopy Core provided
489 imaging assistance, and Elise M. Peaurori provided technical assistance during early stages of
490 this project. We thank members of the Szpara and Weitzman labs for helpful discussions. This

research was supported by NIAID grant 1R21AI140443 (MLS and MDW), with additional support from the following: startup funds from the Pennsylvania State University (MLS), a CURE grant from the Pennsylvania Department of Health (MLS), a grant from the National Institutes of Health (NS082240 to MDW), and the NICHD Pediatric Scientist Development grant K12-HD000850 (LNA). The published NIAID CASG clinical studies of neonatal HSV infection were funded by a contract (N01-AI-62554) with the NIAID Development and Applications Branch and by grants from the General Clinical Research Center Program (RR-032) and the state of Alabama.

Author Contributions

Writing – Original Draft: LNA, CB, AND, and MLS; Writing – Review & Editing: LNA, MDW, and MLS; Conceptualization: LNA and MLS; Investigation: LNA, CB, AND, DWR, UP; Resources: DWK, MNP, and RJW; Funding Acquisition: MLS, RJW, and MDW.

Declaration of Interests

The authors declare no competing interests.

505 # Figure Legends

506 **Figure 1. Neonatal HSV-2 isolates generate different sized plaques in culture.**

507 (**A**) Representative plaques are shown after virus incubation on Vero cells for 100 h. The
508 previously described low-passage adult HSV-2 strain SD90e is shown for comparison (64). Scale
509 bar = 5mm. (**B**) Quantification of plaque area on Vero cells. Dots represent 100 individually
510 measured plaques and black bar represents the mean. Each green isolate (large-plaque) is
511 statistically larger than each black isolate (small-plaque). Black isolates are not statistically
512 different from one another. Additionally, each CSF-derived isolate is statistically larger than all
513 other isolates shown. For all statistics, $p<0.05$ by one-way ANOVA followed by Holm-Sidak's
514 multiple comparisons test.

515 **Figure 2. Increased plaque size in culture is not determined by viral entry, DNA**
516 **replication, protein expression, or infectious virus production.**

517 Viral growth characteristics were compared for representative neonatal isolates, including large-
518 plaque-formers (green) and small-plaque-formers (black). **(A-B)** Viral entry kinetics. **(A)** Viral
519 isolates were applied to Vero cell monolayers at 4°C for 1 h to allow virus binding, then moved
520 to 37°C to allow virus entry. Extracellular virus was inactivated by a low-pH buffer at the times
521 indicated (orange arrowheads). Cell monolayers were washed and overlaid with methylcellulose.
522 Plaques were scored after 100 h of incubation. **(B)** Viral entry was quantified as the fraction of
523 plaques formed following citrate buffer application, where 100% is the number of plaques
524 formed on a monolayer not treated with citrate buffer (control). These data represent three
525 independent experiments. Two-way ANOVA followed by Tukey's multiple comparison test was
526 applied. **(C-E)** Single-cycle viral replication kinetics. Vero cell monolayers were infected at

527 MOI=5 and incubated in the presence of 0.1% human serum. Cell monolayers were harvested at
528 the time points indicated. **(C)** The quantity of viral genomes present was evaluated by qPCR for
529 UL27. Infectious virion production (titer) was evaluated by plaque formation on U2OS **(D)** or
530 Vero **(E)** cells. These data represent three independent experiments. Two-way ANOVA followed
531 by Tukey's multiple comparison test was applied. **(F-G)** Protein production. Vero cell
532 monolayers were infected at MOI=5 for 6 h **(F)** or 24 h **(G)**. Whole cell lysates were subjected to
533 immunoblot analysis with the following antibodies: gC/gD/gE/gH, four virion glycoproteins;
534 VP5 (UL19), capsid protein; ICP8 (UL29), viral single-strand DNA-binding protein; HSV, viral
535 antibody against whole HSV-1; and GAPDH, cellular glyceraldehyde-3 phosphate
536 dehydrogenase as a loading control.

537 **Figure 3. Enhanced viral cell-to-cell spread contributes to increased plaque size in**
538 **culture.**

539 (**A**) The rate of viral spread in Vero cells was compared for representative neonatal isolates,
540 including large-plaque-formers (green) and small-plaque-formers (black). Vero cell monolayers
541 were infected at MOI=0.001 in the presence of 0.1% human serum, which was replenished every
542 24 h. Samples were harvested at each time point and viral titer was evaluated by plaque
543 formation on U2OS cells **(B)** or Vero cells **(C).** These data represent three independent
544 experiments. Two-way ANOVA followed by Tukey's multiple comparison test, *$p<0.0001$ at 72
545 h. **(D)** In parallel experiments, HSV positive cells (green) were evaluated by
546 immunofluorescence. Cell nuclei are counterstained with DAPI (blue). Scale bar = 200 μm.
547 Images are representative of three independent experiments. Images of the entire 10 mm
548 coverslips were then captured and stitched to create a composite image (see **Figure S2**). (**E**) The

549 total number of immunofluorescent (green) pixels was quantified for each coverslip. Two-way
550 ANOVA followed by Tukey's multiple comparison test, *$p<0.05$ at 72 h.

551 **Figure 4. Neonatal HSV-2 genomes are genetically distinct from one another and**
552 **encompass a broad range of known HSV-2 genetic diversity.**

553 A phylogenetic network constructed among neonatal HSV-2 genomes (**A**), or neonatal and adult
554 HSV-2 genomes (**B**), reveals the wide genetic distribution of these unrelated isolates. HSV-2
555 genomes have been previously noted to lack geographic separation into clades (41, 42, 82). The
556 network was created using SplitsTree4, from a MAFFT trimmed genome alignment. See **Figure**
557 **S3** for a comparison tree constructed using a neighbor-joining (NJ) algorithm. See **Table S1** for a
558 complete list of accessions, geographic origins, and references for all 58 adult HSV2 strains.

559 **Figure 5: Neonatal HSV-2 proteins contain a similar degree of consensus-level**
560 **amino acid (AA) differences as adult HSV-2 isolates.**

561 HSV-2 proteins are grouped by function, and the percentage of variable AAs in each protein
562 (#AA differences divided by protein length) are plotted for the 10 neonatal isolates (dark blue),
563 for 10 representative adult HSV-2 isolates (light blue), and for all 58 annotated adult HSV-2
564 genomes in GenBank (clear outlines behind light blue boxes). All adult HSV-2 genomes used for
565 this comparison are listed in **Table S1**.

566 **Figure 6: Minority variants expand the range of neonatal HSV-2 coding diversity.**

567 (**A**) Scatter plot indicates the total number of minor variants (MV; y-axis) observed in each
568 neonatal isolate. MV are rare alleles that exist within each viral population, below the level of the

569 consensus genome. The total number of MV on the left is separated into single-nucleotide
570 polymorphism (SNP) vs. insertion/deletion (INDEL) variants on the right (x-axis). The genomic
571 location of each SNP or INDEL variant is also summarized: intergenic vs. inside of genes (genic)
572 for INDELS, and intergenic vs. nonsynonymous or synonymous SNPs inside of genes. (**B**) The
573 frequency, or penetrance, of each minority variant was examined for each isolate. Data (x-axis)
574 was binned in increments of 5% (e.g. 0-<5% frequency, 5-<10% frequency, and so on), and
575 plotted according to the number of MV observed at each frequency (y-axis). SNP and INDEL
576 variants were combined for this analysis. (**C**) Stacked histograms show the number of genic MV
577 (x-axis) located in each HSV-2 coding sequence (gene; y-axis). SNP and INDEL variants were
578 combined for this analysis. UL3, UL11, UL35, and UL55 lacked any minority variants and are
579 not included in the histogram. See **Table S3** for full list of SNP and INDEL MV position and
580 frequency data.

581 **Figure 7. Coding variations identified in neonatal HSV-2 isolates in proteins known**
582 **to contribute to cell-to-cell spread and neurovirulence.**

583 The domain structure of each HSV protein is based on published literature for both HSV-1 and -
584 2. Red arrows indicate protein-coding variations discussed in the text, with the BLOSUM80
585 score for each AA substitution listed in parenthesis beneath the highlighted difference. More
586 detailed information regarding cell-to-cell spread and neurovirulence can be found in **Table S4**.

587

588 # References

589 1. Looker KJ, Magaret AS, May MT, Turner KM, Vickerman P, Newman LM, Gottlieb SL.
590 2017. First estimates of the global and regional incidence of neonatal herpes infection.
591 Lancet Glob Health 5:e300–e309.

592 2. Stephenson-Famy A, Gardella C. 2014. Herpes Simplex Virus Infection During Pregnancy.
593 Obstet Gynecol Clin North Am 41:601–614.

594 3. Brown ZA, Wald A, Morrow RA, Selke S, Zeh J, Corey L. 2003. Effect of serologic status
595 and cesarean delivery on transmission rates of herpes simplex virus from mother to infant.
596 Jama 289:203–209.

597 4. Corey L, Wald A. 2009. Maternal and Neonatal HSV Infections. N Engl J Med 361:1376–
598 1385.

599 5. Bradley H, Markowitz LE, Gibson T, McQuillan GM. 2014. Seroprevalence of herpes
600 simplex virus types 1 and 2--United States, 1999-2010. J Infect Dis 209:325–333.

601 6. James SH, Kimberlin DW. 2014. Neonatal Herpes Simplex Virus Infection. Clin Perinatol.

602 7. Pinninti SG, Kimberlin DW. 2014. Preventing Herpes Simplex Virus in the Newborn. Clin
603 Perinatol 41:945–955.

604 8. Kimberlin DW, Lin CY, Jacobs RF, Powell DA, Frenkel LM, Gruber WC, Rathore M,
605 Bradley JS, Diaz PS, Kumar M, Arvin AM, Gutierrez K, Shelton M, Weiner LB, Sleasman
606 JW, de Sierra TM, Soong SJ, Kiell J, Lakeman FD, Whitley RJ, National Institute of
607 Allergy and Infectious Diseases Collaborative Antiviral Study Group. 2001. Natural history
608 of neonatal herpes simplex virus infections in the acyclovir era. Pediatrics 108:223–229.

609 9. Kimberlin DW, Whitley RJ, Wan W, Powell DA, Storch G, Ahmed A, Palmer A, Sánchez
610 PJ, Jacobs RF, Bradley JS. 2011. Oral acyclovir suppression and neurodevelopment after
611 neonatal herpes. N Engl J Med 365:1284–1292.

612 10. Casanova J-L. 2015. Human genetic basis of interindividual variability in the course of
613 infection. Proc Natl Acad Sci 201521644.

614 11. Zhang S-Y, Jouanguy E, Ugolini S, Smahi A, Elain G, Romero P, Segal D, Sancho-Shimizu
615 V, Lorenzo L, Puel A, Picard C, Chapgier A, Plancoulaine S, Titeux M, Cognet C, von
616 Bernuth H, Ku C-L, Casrouge A, Zhang X-X, Barreiro L, Leonard J, Hamilton C, Lebon P,
617 Heron B, Vallee L, Quintana-Murci L, Hovnanian A, Rozenberg F, Vivier E, Geissmann F,
618 Tardieu M, Abel L, Casanova J-L. 2007. TLR3 deficiency in patients with herpes simplex
619 encephalitis. Science 317:1522–1527.

620 12. Whitley R, Arvin A, Prober C, Corey L, Burchett S, Plotkin S, Starr S, Jacobs R, Powell D,
621 Nahmias A, Sumaya C, Edwards K, Alford C, Caddell G, Soong S-J, the National Institute
622 of Allergy and Infectious Diseases Collaborative Antiviral Study Group*. 1991. Predictors
623 of Morbidity and Mortality in Neonates with Herpes Simplex Virus Infections. N Engl J
624 Med 324:450–454.

625 13. Fields BN, Byers K. 1983. The Genetic Basis of Viral Virulence. Philos Trans R Soc Lond B
626 Biol Sci 303:209–218.

627 14. Gonzalez-Scarano F, Beaty B, Sundin D, Janssen R, Endres MJ, Nathanson N. 1988. Genetic
628 determinants of the virulence and infectivity of La Crosse virus. Microb Pathog 4:1–7.

629 15. Tscherne DM, García-Sastre A. 2011. Virulence determinants of pandemic influenza viruses.
630 J Clin Invest 121:6–13.

631 16. Müller V, Fraser C, Herbeck JT. 2011. A Strong Case for Viral Genetic Factors in HIV
632 Virulence. Viruses 3:204–216.

633 17. Robinson CM, Jesudhasan PR, Pfeiffer JK. 2014. Bacterial Lipopolysaccharide Binding
634 Enhances Virion Stability and Promotes Environmental Fitness of an Enteric Virus. Cell
635 Host Microbe 15:36–46.

636 18. Yoshii K, Sunden Y, Yokozawa K, Igarashi M, Kariwa H, Holbrook MR, Takashima I.
637 2014. A Critical Determinant of Neurological Disease Associated with Highly Pathogenic
638 Tick-Borne Flavivirus in Mice. J Virol 88:5406–5420.

639 19. Roizman B, Whitley RJ. 2001. The nine ages of herpes simplex virus. Herpes 8:23–27.

640 20. Sakaoka H, Kawana T, Grillner L, Aomori T, Yamiguchi T, Saito H, Fujinaga K. 1987.
641 Genome Variations in Herpes Simplex Virus Type 2 Strains Isolated in Japan and Sweden.
642 J Gen Virol 68:2105–16.

643 21. Sakaoka H, Kurita K, Iida Y, Takada S, Umene K, Kim YT, Ren CS, Nahmias AJ. 1994.
644 Quantitative analysis of genomic polymorphism of herpes simplex virus type 1 strains from
645 six countries: studies of molecular evolution and molecular epidemiology of the virus. J
646 Gen Virol 75:513–27.

647 22. Bowden R, Sakaoka H, Ward R, Donnelly P. 2006. Patterns of Eurasian HSV-1 molecular
648 diversity and inferences of human migrations. Infect Genet Evol 6:63–74.

649 23. Bower JR, Mao H, Durishin C, Rozenbom E, Detwiler M, Rempinski D, Karban TL,
650 Rosenthal KS. 1999. Intrastrain variants of herpes simplex virus type 1 isolated from a
651 neonate with fatal disseminated infection differ in the ICP34.5 gene, glycoprotein
652 processing, and neuroinvasiveness. J Virol 73:3843–53.

653 24. Mao H, Rosenthal KS. 2003. Strain-Dependent Structural Variants of Herpes Simplex Virus
654 Type 1 ICP34.5 Determine Viral Plaque Size, Efficiency of Glycoprotein Processing, and
655 Viral Release and Neuroinvasive Disease Potential. J Virol 77:3409–3417.

656 25. Renzette N, Gibson L, Jensen JD, Kowalik TF. 2014. Human cytomegalovirus intrahost
657 evolution—a new avenue for understanding and controlling herpesvirus infections. Curr
658 Opin Virol 8:109–115.

659 26. Depledge DP, Kundu S, Jensen NJ, Gray ER, Jones M, Steinberg S, Gershon A, Kinchington
660 PR, Schmid DS, Balloux F, Nichols RA, Breuer J. 2014. Deep Sequencing of Viral
661 Genomes Provides Insight into the Evolution and Pathogenesis of Varicella Zoster Virus
662 and Its Vaccine in Humans. Mol Biol Evol 31:397–409.

663 27. Renner DW, Szpara ML. 2018. The impacts of genome-wide analyses on our understanding
664 of human herpesvirus diversity and evolution. J Virol 92:e00908-17.

665 28. Houldcroft CJ, Bryant JM, Depledge DP, Margetts BK, Simmonds J, Nicolaou S, Tutill HJ,
666 Williams R, Worth AJJ, Marks SD, Veys P, Whittaker E, Breuer J. 2016. Detection of Low
667 Frequency Multi-Drug Resistance and Novel Putative Maribavir Resistance in
668 Immunocompromised Pediatric Patients with Cytomegalovirus. Front Microbiol 7.

669 29. Houldcroft CJ, Beale MA, Breuer J. 2017. Clinical and biological insights from viral genome
670 sequencing. Nat Rev Microbiol 15:183–192.

671 30. Renzette N, Bhattacharjee B, Jensen JD, Gibson L, Kowalik TF. 2011. Extensive genome-
672 wide variability of human cytomegalovirus in congenitally infected infants. PLoS Pathog
673 7:1–14.

674 31. Renzette N, Gibson L, Bhattacharjee B, Fisher D, Schleiss MR, Jensen JD, Kowalik TF.
675 2013. Rapid intrahost evolution of human cytomegalovirus is shaped by demography and
676 positive selection. PLoS Genet 9:1–14.

677 32. Renzette N, Pokalyuk C, Gibson L, Bhattacharjee B, Schleiss MR, Hamprecht K, Yamamoto
678 AY, Mussi-Pinhata MM, Britt WJ, Jensen JD, Kowalik TF. 2015. Limits and patterns of
679 cytomegalovirus genomic diversity in humans. Proc Natl Acad Sci 201501880.

680 33. Renzette N, Kowalik TF, Jensen JD. 2016. On the relative roles of background selection and
681 genetic hitchhiking in shaping human cytomegalovirus genetic diversity. Mol Ecol 25:403–
682 413.

683 34. Renzette N, Pfeifer SP, Matuszewski S, Kowalik TF, Jensen JD. 2017. On the Analysis of
684 Intrahost and Interhost Viral Populations: Human Cytomegalovirus as a Case Study of
685 Pitfalls and Expectations. J Virol 91:e01976-16.

686 35. Pokalyuk C, Renzette N, Irwin KK, Pfeifer SP, Gibson L, Britt WJ, Yamamoto AY, Mussi-
687 Pinhata MM, Kowalik TF, Jensen JD. 2017. Characterizing human cytomegalovirus
688 reinfection in congenitally infected infants: an evolutionary perspective. Mol Ecol.

689 36. Sijmons S, Van Ranst M, Maes P. 2014. Genomic and Functional Characteristics of Human
690 Cytomegalovirus Revealed by Next-Generation Sequencing. Viruses 6:1049–1072.

691 37. Sijmons S, Thys K, Mbong Ngwese M, Van Damme E, Dvorak J, Van Loock M, Li G,
692 Tachezy R, Busson L, Aerssens J, Van Ranst M, Maes P. 2015. High-Throughput Analysis
693 of Human Cytomegalovirus Genome Diversity Highlights the Widespread Occurrence of
694 Gene-Disrupting Mutations and Pervasive Recombination. J Virol 89:7673–7695.

695 38. Lassalle F, Depledge DP, Reeves MB, Brown AC, Christiansen MT, Tutill HJ, Williams RJ,
696 Einer-Jensen K, Holdstock J, Atkinson C, Brown JR, van Loenen FB, Clark DA, Griffiths
697 PD, Verjans GMGM, Schutten M, Milne RSB, Balloux F, Breuer J. 2016. Islands of
698 linkage in an ocean of pervasive recombination reveals two-speed evolution of human
699 cytomegalovirus genomes. Virus Evol 2:vew017.

700 39. Johnston C, Magaret A, Roychoudhury P, Greninger AL, Reeves D, Schiffer J, Jerome KR,
701 Sather C, Diem K, Lingappa JR, Celum C, Koelle DM, Wald A. 2017. Dual-strain genital
702 herpes simplex virus type 2 (HSV-2) infection in the US, Peru, and 8 countries in sub-

703 Saharan Africa: A nested cross-sectional viral genotyping study. PLOS Med 14:e1002475.

704 40. Minaya MA, Jensen TL, Goll JB, Korom M, Datla SH, Belshe RB, Morrison LA. 2017.
705 Molecular evolution of herpes simplex virus 2 complete genomes: comparison between
706 primary and recurrent infections. J Virol 91:e00942–17.

707 41. Koelle DM, Norberg P, Fitzgibbon MP, Russell RM, Greninger AL, Huang M-L, Stensland
708 L, Jing L, Magaret AS, Diem K, Selke S, Xie H, Celum C, Lingappa JR, Jerome KR, Wald
709 A, Johnston C. 2017. Worldwide circulation of HSV-2 × HSV-1 recombinant strains. Sci
710 Rep 7:44084.

711 42. Burrel S, Boutolleau D, Ryu D, Agut H, Merkel K, Leendertz FH, Calvignac-Spencer S.
712 2017. Ancient Recombination Events between Human Herpes Simplex Viruses. Mol Biol
713 Evol 34:1713–1721.

714 43. Ryncarz AJ, Goddard J, Wald A, Huang M-L, Roizman B, Corey L. 1999. Development of a
715 high-throughput quantitative assay for detecting herpes simplex virus DNA in clinical
716 samples. J Clin Microbiol 37:1941–1947.

717 44. Wald A, Huang M-L, Carrell D, Selke S, Corey L. 2003. Polymerase chain reaction for
718 detection of herpes simplex virus (HSV) DNA on mucosal surfaces: comparison with HSV
719 isolation in cell culture. J Infect Dis 188:1345–1351.

720 45. Szpara ML, Tafuri YR, Parsons L, Shamim SR, Verstrepen KJ, Legendre M, Enquist LW.
721 2011. A wide extent of inter-strain diversity in virulent and vaccine strains of
722 alphaherpesviruses. PLoS Pathog 7:1–23.

723 46. Brown J. 2004. Effect of gene location on the evolutionary rate of amino acid substitutions in
724 herpes simplex virus proteins. Virology 330:209–20.

725 47. Bowden R, Sakaoka H, Donnelly P, Ward R. 2004. High recombination rate in herpes
726 simplex virus type 1 natural populations suggests significant co-infection. Infect Genet Evol
727 4:115–23.

728 48. Norberg P, Bergstrom T, Rekabdar E, Lindh M. 2004. Phylogenetic Analysis of Clinical
729 Herpes Simplex Virus Type 1 Isolates Identified Three Genetic Groups and Recombinant
730 Viruses. J Virol 78:10755–10764.

731 49. Norberg P, Kasubi MJ, Haarr L, Bergstrom T, Liljeqvist J-A. 2007. Divergence and
732 recombination of clinical herpes simplex virus type 2 isolates. J Virol 81:13158–13167.

733 50. Lonsdale DM, Brown SM, Lang J, Subak-Sharpe JH, Koprowski H, Warren KG. 1980.
734 Variations in herpes simplex virus isolated from human ganglia and a study of clonal
735 variation in HSV-1. Ann N Y Acad Sci 291–308.

736 51. Liljeqvist JA, Tunback P, Norberg P. 2009. Asymptomatically shed recombinant herpes
737 simplex virus type 1 strains detected in saliva. J Gen Virol 90:559–566.

738 52. Haarr L, Nilsen A, Knappskog PM, Langeland N. 2014. Stability of glycoprotein gene
739 sequences of herpes simplex virus type 2 from primary to recurrent human infection, and
740 diversity of the sequences among patients attending an STD clinic. BMC Infect Dis 14:63.

741 53. Szpara ML, Gatherer D, Ochoa A, Greenbaum B, Dolan A, Bowden RJ, Enquist LW,
742 Legendre M, Davison AJ. 2014. Evolution and diversity in human herpes simplex virus
743 genomes. J Virol 88:1209–27.

744 54. Parsons LR, Tafuri YR, Shreve JT, Bowen CD, Shipley MM, Enquist LW, Szpara ML.
745 2015. Rapid genome assembly and comparison decode intrastrain variation in human
746 alphaherpesviruses. mBio 6:e02213-14.

747 55. Kolb AW, Lee K, Larsen I, Craven M, Brandt CR. 2016. Quantitative Trait Locus Based
748 Virulence Determinant Mapping of the HSV-1 Genome in Murine Ocular Infection: Genes
749 Involved in Viral Regulatory and Innate Immune Networks Contribute to Virulence. PLOS
750 Pathog 12:e1005499.

751 56. Pfaff F, Groth M, Sauerbrei A, Zell R. 2016. Genotyping of herpes simplex virus type 1
752 (HSV-1) by whole genome sequencing. J Gen Virol.

753 57. Bowen CD, Renner DW, Shreve JT, Tafuri Y, Payne KM, Dix RD, Kinchington PR,
754 Gatherer D, Szpara ML. 2016. Viral forensic genomics reveals the relatedness of classic
755 herpes simplex virus strains KOS, KOS63, and KOS79. Virology 492:179–186.

756 58. Pandey U, Renner DW, Thompson RL, Szpara ML, Sawtell NM. 2017. Inferred father-to-
757 son transmission of herpes simplex virus results in near-perfect preservation of viral
758 genome identity and in vivo phenotypes. Sci Rep 7:13666.

759 59. Szpara ML, Parsons L, Enquist LW. 2010. Sequence variability in clinical and laboratory
760 isolates of herpes simplex virus 1 reveals new mutations. J Virol 84:5303–13.

761 60. Parsons LR, Tafuri YR, Shreve JT, Bowen CD, Shipley MM, Enquist LW, Szpara ML.
762 2015. Rapid genome assembly and comparison decode intrastrain variation in human
763 alphaherpesviruses. mBio 6:e02213-14.

764 61. Kimberlin DW, Lin CY, Jacobs RF, Powell DA, Corey L, Gruber WC, Rathore M, Bradley
765 JS, Diaz PS, Kumar M, Arvin AM, Gutierrez K, Shelton M, Weiner LB, Sleasman JW, de
766 Sierra TM, Weller S, Soong SJ, Kiell J, Lakeman FD, Whitley RJ, National Institute of
767 Allergy and Infectious Diseases Collaborative Antiviral Study Group. 2001. Safety and
768 efficacy of high-dose intravenous acyclovir in the management of neonatal herpes simplex
769 virus infections. Pediatrics 108:230–238.

770 62. Desmyter J, Melnick JL, Rawls WE. 1968. Defectiveness of interferon production and of
771 rubella virus interference in a line of African green monkey kidney cells (Vero). J Virol
772 2:955–961.

773 63. Emeny JM, Morgan MJ. 1979. Regulation of the interferon system: evidence that Vero cells
774 have a genetic defect in interferon production. J Gen Virol 43:247–252.

775 64. Colgrove R, Diaz F, Newman R, Saif S, Shea T, Young S, Henn M, Knipe DM. 2014.
776 Genomic sequences of a low passage herpes simplex virus 2 clinical isolate and its plaque-
777 purified derivative strain. Virology 450–451:140–145.

778 65. Yao F, Schaffer PA. 1995. An activity specified by the osteosarcoma line U2OS can
779 substitute functionally for ICP0, a major regulatory protein of herpes simplex virus type 1. J
780 Virol 69:6249–6258.

781 66. Deschamps T, Kalamvoki M. 2017. Impaired STING Pathway in Human Osteosarcoma
782 U2OS Cells Contributes to the Growth of ICP0-Null Mutant Herpes Simplex Virus. J Virol
783 91:e00006-17.

784 67. Norberg P. 2010. Divergence and genotyping of human alpha-herpesviruses: an overview.
785 Infect Genet Evol J Mol Epidemiol Evol Genet Infect Dis 10:14–25.

786 68. David AT, Saied A, Charles A, Subramanian R, Chouljenko VN, Kousoulas KG. 2012. A
787 Herpes Simplex Virus 1 (McKrae) Mutant Lacking the Glycoprotein K Gene Is Unable To
788 Infect via Neuronal Axons and Egress from Neuronal Cell Bodies. mBio 3.

789 69. Dingwell KS, Brunetti CR, Hendricks RL, Tang Q, Tang M, Rainbow AJ, Johnson DC.
790 1994. Herpes simplex virus glycoproteins E and I facilitate cell-to-cell spread in vivo and
791 across junctions of cultured cells. J Virol 68:834–845.

792 70. Weber PC, Levine M, Glorioso JC. 1987. Rapid identification of nonessential genes of
793 herpes simplex virus type 1 by Tn5 mutagenesis. Science 236:576–579.

794 71. Jacobson JG, Martin SL, Coen DM. 1989. A conserved open reading frame that overlaps the
795 herpes simplex virus thymidine kinase gene is important for viral growth in cell culture. J
796 Virol 63:1839–1843.

797 72. Foster TP, Melancon JM, Baines JD, Kousoulas KG. 2004. The herpes simplex virus type 1
798 UL20 protein modulates membrane fusion events during cytoplasmic virion morphogenesis
799 and virus-induced cell fusion. J Virol 78:5347–5357.

800 73. David AT, Baghian A, Foster TP, Chouljenko VN, Kousoulas KG. 2008. The herpes simplex
801 virus type 1 (HSV-1) glycoprotein K(gK) is essential for viral corneal spread and
802 neuroinvasiveness. Curr Eye Res 33:455–467.

803 74. Dingwell KS, Johnson DC. 1998. The herpes simplex virus gE-gI complex facilitates cell-to-
804 cell spread and binds to components of cell junctions. J Virol 72:8933–8942.

805 75. Meignier B, Longnecker R, Mavromara-Nazos P, Sears AE, Roizman B. 1988. Virulence of
806 and establishment of latency by genetically engineered deletion mutants of herpes simplex
807 virus 1. Virology 162:251–254.

808 76. Rochette P-A, Bourget A, Sanabria-Solano C, Lahmidi S, Lavallée GO, Pearson A. 2015.
809 Mutation of UL24 impedes the dissemination of acute herpes simplex virus 1 infection
810 from the cornea to neurons of trigeminal ganglia. J Gen Virol 96:2794–2805.

811 77. Jacobson JG, Chen SH, Cook WJ, Kramer MF, Coen DM. 1998. Importance of the herpes
812 simplex virus UL24 gene for productive ganglionic infection in mice. Virology 242:161–
813 169.

814 78. Leiva-Torres GA, Rochette P-A, Pearson A. 2010. Differential importance of highly
815 conserved residues in UL24 for herpes simplex virus 1 replication in vivo and reactivation.
816 J Gen Virol 91:1109–1116.

817 79. Liu J, Lewin AS, Tuli SS, Ghivizzani SC, Schultz GS, Bloom DC. 2008. Reduction in
818 severity of a herpes simplex virus type 1 murine infection by treatment with a ribozyme
819 targeting the UL20 gene RNA. J Virol 82:7467–7474.

820 80. Newman RM, Lamers SL, Weiner B, Ray SC, Colgrove RC, Diaz F, Jing L, Wang K, Saif S,
821 Young S, Henn M, Laeyendecker O, Tobian AAR, Cohen JI, Koelle DM, Quinn TC, Knipe
822 DM. 2015. Genome Sequencing and Analysis of Geographically Diverse Clinical Isolates
823 of Herpes Simplex Virus 2. J Virol JVI.01303-15.

824 81. Kolb AW, Larsen IV, Cuellar JA, Brandt CR. 2015. Genomic, Phylogenetic, and
825 Recombinational Characterization of Herpes Simplex Virus 2 Strains. J Virol 89:6427–
826 6434.

827 82. Johnston C, Magaret A, Roychoudhury P, Greninger AL, Cheng A, Diem K, Fitzgibbon MP,
828 Huang M, Selke S, Lingappa JR, Celum C, Jerome KR, Wald A, Koelle DM. 2017. Highly
829 conserved intragenic HSV-2 sequences: Results from next-generation sequencing of HSV-2
830 U L and U S regions from genital swabs collected from 3 continents. Virology 510:90–98.

831 83. Minaya MA, Jensen T, Goll J, Korom M, Datla SH, Belshe RB, Morrison LA. 2017.
832 Molecular evolution of herpes simplex virus 2 complete genomes: Comparison between
833 primary and recurrent infections. J Virol JVI.00942-17.

834 84. Whitley R, Arvin A, Prober C, Burchett S, Corey L, Powell D, Plotkin S, Starr S, Alford C,
835 Connor J, Jacobs R, Nahmias A, Soong S-J, the National Institute of Allergy, Infectious
836 Diseases Collaborative Antiviral Study Group*. 1991. A Controlled Trial Comparing
837 Vidarabine with Acyclovir in Neonatal Herpes Simplex Virus Infection. N Engl J Med
838 324:444–449.

839 85. Avgousti DC, Della Fera AN, Otter CJ, Herrmann C, Pancholi NJ, Weitzman MD. 2017.
840 Adenovirus Core Protein VII Downregulates the DNA Damage Response on the Host
841 Genome. J Virol 91:e01089-17.

842 86. Szpara ML, Tafuri YR, Enquist LW. 2011. Preparation of viral DNA from nucleocapsids. J
843 Vis Exp JoVE 2–7.

844 87. Szpara M. 2014. Isolation of herpes simplex virus nucleocapsid DNA, p. 31–41. *In*
845 Diefenbach, RJ, Fraefel, C (eds.), Herpes Simplex Virus. Springer New York, New York,
846 NY.

847 88. Bowen CD, Renner DW, Shreve JT, Tafuri Y, Payne KM, Dix RD, Kinchington PR,
848 Gatherer D, Szpara ML. 2016. Viral forensic genomics reveals the relatedness of classic
849 herpes simplex virus strains KOS, KOS63, and KOS79. Virology 492:179–186.

850 89. Dolan A, Jamieson FE, Cunningham C, Barnett BC, McGeoch DJ. 1998. The genome
851 sequence of herpes simplex virus type 2. J Virol 72:2010–2021.

852 90. Katoh K, Misawa K, Kuma K, Miyata T. 2002. MAFFT: a novel method for rapid multiple
853 sequence alignment based on fast Fourier transform. Nucleic Acids Res 30:3059–3066.

854 91. Strimmer K, Wiuf C, Moulton V. 2001. Recombination analysis using directed graphical
855 models. Mol Biol Evol 18:97–99.

856 92. Norberg P, Tyler S, Severini A, Whitley R, Liljeqvist J-A, Bergstrom T. 2011. A genome-
857 wide comparative evolutionary analysis of herpes simplex virus type 1 and varicella zoster
858 virus. PloS One 6:1–8.

859 93. Tamura K, Stecher G, Peterson D, Filipski A, Kumar S. 2013. MEGA6: Molecular
860 Evolutionary Genetics Analysis Version 6.0. Mol Biol Evol 30:2725–2729.

861 94. Larkin MA, Blackshields G, Brown NP, Chenna R, McGettigan PA, McWilliam H, Valentin
862 F, Wallace IM, Wilm A, Lopez R, Thompson JD, Gibson TJ, Higgins DG. 2007. Clustal W
863 and Clustal X version 2.0. Bioinforma Appl Note 23:2947–2948.

864 95. Koboldt DC, Zhang Q, Larson DE, Shen D, McLellan MD, Lin L, Miller CA, Mardis ER,
865 Ding L, Wilson RK. 2012. VarScan 2: Somatic mutation and copy number alteration
866 discovery in cancer by exome sequencing. Genome Res 22:568–576.

867 96. Cingolani P, Platts A, Wang LL, Coon M, Nguyen T, Wang L, Land SJ, Lu X, Ruden DM.
868 2012. A program for annotating and predicting the effects of single nucleotide
869 polymorphisms, SnpEff. Fly (Austin) 6:80–92.

870 97. Cingolani P, Patel VM, Coon M, Nguyen T, Land SJ, Ruden DM, Lu X. 2012. Using
871 Drosophila melanogaster as a Model for Genotoxic Chemical Mutational Studies with a
872 New Program, SnpSift. Front Genet 3.

873 98. Depledge DP, Yamanishi K, Gomi Y, Gershon AA, Breuer J. 2016. Deep Sequencing of
874 Distinct Preparations of the Live Attenuated Varicella-Zoster Virus Vaccine Reveals a
875 Conserved Core of Attenuating Single-Nucleotide Polymorphisms. J Virol 90:8698–8704.

876 99. Hage E, Wilkie GS, Linnenweber-Held S, Dhingra A, Suárez NM, Schmidt JJ, Kay-Fedorov
877 PC, Mischak-Weissinger E, Heim A, Schwarz A, Schulz TF, Davison AJ, Ganzenmueller
878 T. 2017. Characterization of Human Cytomegalovirus Genome Diversity in
879 Immunocompromised Hosts by Whole-Genome Sequencing Directly From Clinical
880 Specimens. J Infect Dis 215:1673–1683.

881

882 # Tables

883 **Table 1: Clinical characteristics associated with HSV-2 isolates from ten patients.**

Clinical Isolate*	Clinical Disease at Diagnosis	Sample Source	Morbidity Score - Mental	Morbidity Score - Motor	Patient Age at Disease Onset (days)	Gestational Age at Time of Birth (weeks)	Patient Sex & Race
CNS11	CNS	CSF	4	4	12	37	M, W
DISS14	DISS + CNS	CSF	2	2	7	39	M, W
CNS03	CNS	SKIN	4	4	17	37	M, W
CNS15	CNS	SKIN	3	4	19	36	M, W
CNS17	CNS	SKIN	4	4	17	40	M, W
DISS29	DISS + CNS	SKIN	3	3	5	38	F, B
CNS12	CNS	SKIN	4	4	16	41	F, W
SEM02	SEM	SKIN	1	1	5	38	F, W
SEM13	SEM	SKIN	4	4	11	27	F, B
SEM18	SEM	SKIN	2	2	17	37	F, W

884 * Clinical isolate order based on **Figure 1**.

885

886

887 **Table 2. Genome sequencing statistics for neonatal HSV-2 strains.**

Clinical Isolate*	Average Coverage	Raw Sequence Reads	Used for Assembly**	% viral	Depth > 100	GenBank Accession
CNS11	6,081X	3.5 million	2.8 million	79%	96%	In process^
DISS14	6,267X	3.8 million	3.0 million	77%	97%	In process^
CNS03	6,269X	3.9 million	3.1 million	78%	96%	In process^
CNS15	7,486X	6.1 million	4.4 million	73%	97%	In process^
CNS17	5,059X	3.1 million	2.3 million	73%	96%	In process^
DISS29	2,588X	1.4 million	1.1 million	78%	99%	In process^
CNS12	5,839X	3.9 million	2.8 million	73%	96%	In process^
SEM02	6,455X	4.8 million	3.7 million	77%	95%	In process^
SEM13	5,291X	3.4 million	2.4 million	72%	89%	In process^
SEM18	7,514X	16.9 million	12.2 million	72%	98%	In process^

888 * Clinical isolate order based on **Figure 1**.
889 ** Numbers reflect the count of sequence read 1 of paired-end reads.
890 ^ GenBank accessions are in process. See “Related Manuscript File” uploaded for review,
891 which contains all 10 GenBank flatfiles.

892

Figures

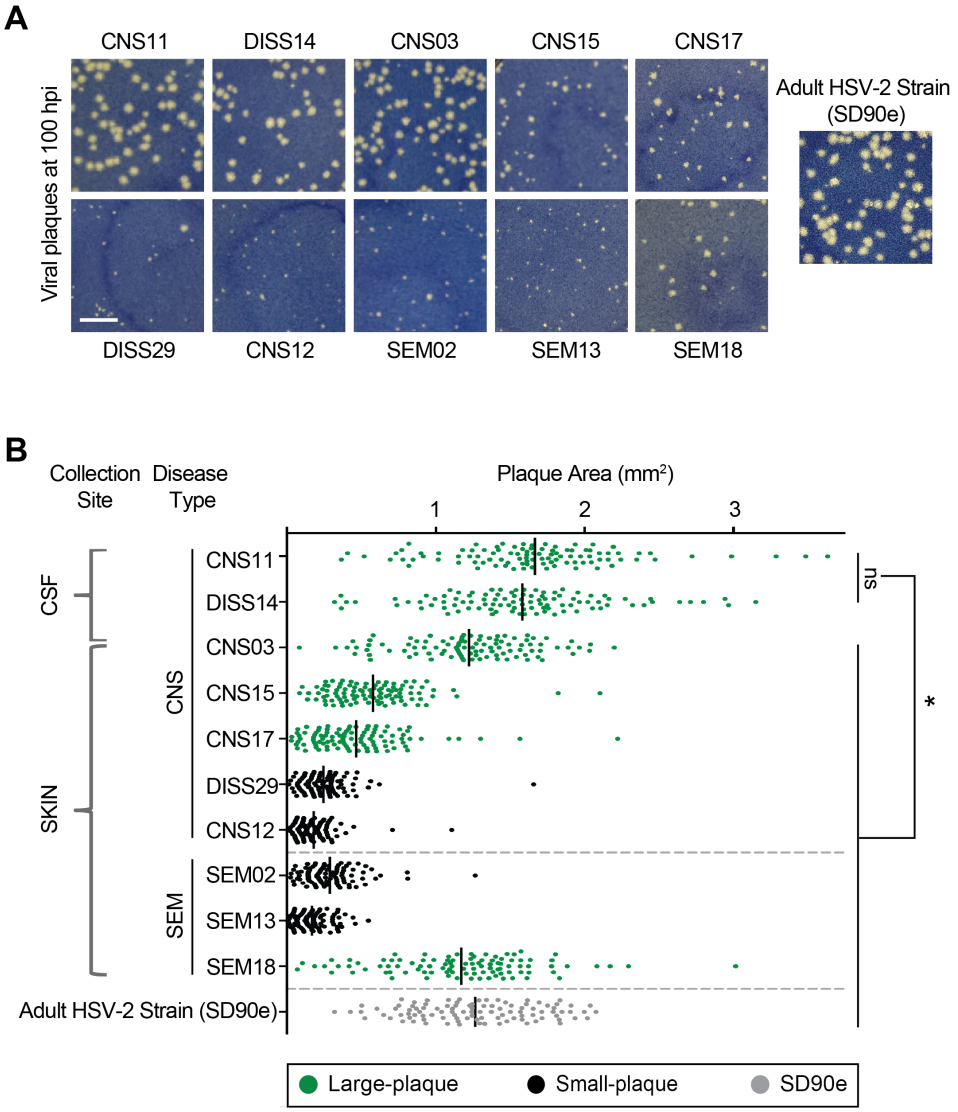

Figure 1. Neonatal HSV-2 isolates generate different sized plaques in culture. (**A**) Representative plaques are shown after virus incubation on Vero cells for 100 h. The previously described low-passage adult HSV-2 strain SD90e is shown for comparison (64). Scale bar = 5mm. (**B**) Quantification of plaque area on Vero cells. Dots represent 100 individually measured plaques and black bar represents the mean. Each green isolate (large-plaque) is statistically larger than each black isolate (small-plaque). Black isolates are not statistically different from one another. Additionally, each CSF-derived isolate is statistically larger than all other isolates shown. For all statistics, $p<0.05$ by one-way ANOVA followed by Holm-Sidak's multiple comparisons test.

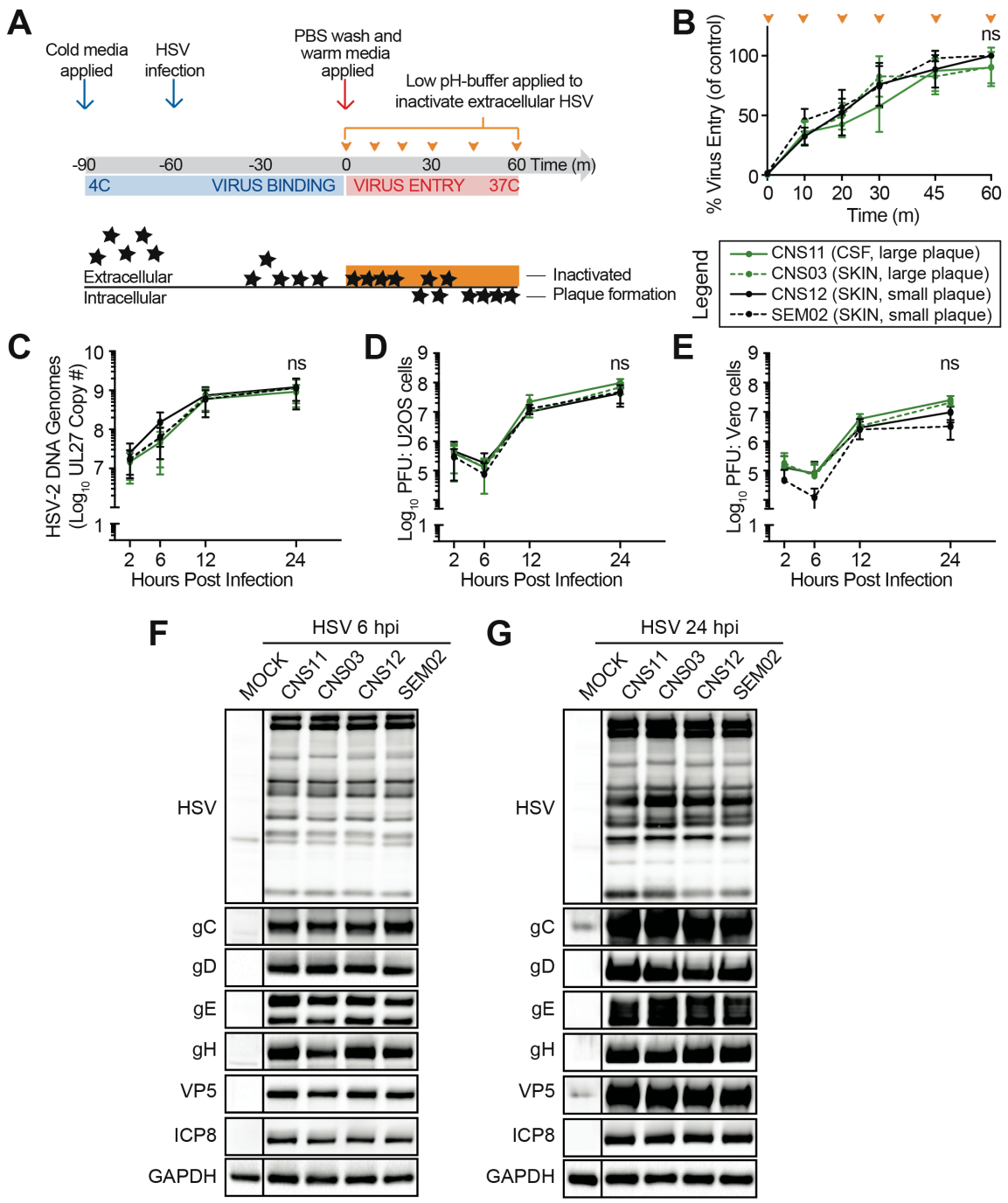

Figure 2. Increased plaque size in culture is not determined by viral entry, DNA replication, protein expression, or infectious virus production.

Viral growth characteristics were compared for representative neonatal isolates, including large-plaque-formers (green) and small-plaque-formers (black). **(A-B)** Viral entry kinetics. **(A)** Viral

909 isolates were applied to Vero cell monolayers at 4°C for 1 h to allow virus binding, then moved
910 to 37°C to allow virus entry. Extracellular virus was inactivated by a low-pH buffer at the times
911 indicated (orange arrowheads). Cell monolayers were washed and overlaid with methylcellulose.
912 Plaques were scored after 100 h of incubation. **(B)** Viral entry was quantified as the fraction of
913 plaques formed following citrate buffer application, where 100% is the number of plaques
914 formed on a monolayer not treated with citrate buffer (control). These data represent three
915 independent experiments. Two-way ANOVA followed by Tukey's multiple comparison test was
916 applied. **(C-E)** Single-cycle viral replication kinetics. Vero cell monolayers were infected at
917 MOI=5 and incubated in the presence of 0.1% human serum. Cell monolayers were harvested at
918 the time points indicated. **(C)** The quantity of viral genomes present was evaluated by qPCR for
919 UL27. Infectious virion production (titer) was evaluated by plaque formation on U2OS **(D)** or
920 Vero **(E)** cells. These data represent three independent experiments. Two-way ANOVA followed
921 by Tukey's multiple comparison test was applied. **(F-G)** Protein production. Vero cell
922 monolayers were infected at MOI=5 for 6 h **(F)** or 24 h **(G)**. Whole cell lysates were subjected to
923 immunoblot analysis with the following antibodies: gC/gD/gE/gH, four virion glycoproteins;
924 VP5 (UL19), capsid protein; ICP8 (UL29), viral single-strand DNA-binding protein; HSV, viral
925 antibody against whole HSV-1; and GAPDH, cellular glyceraldehyde-3 phosphate
926 dehydrogenase as a loading control.

927

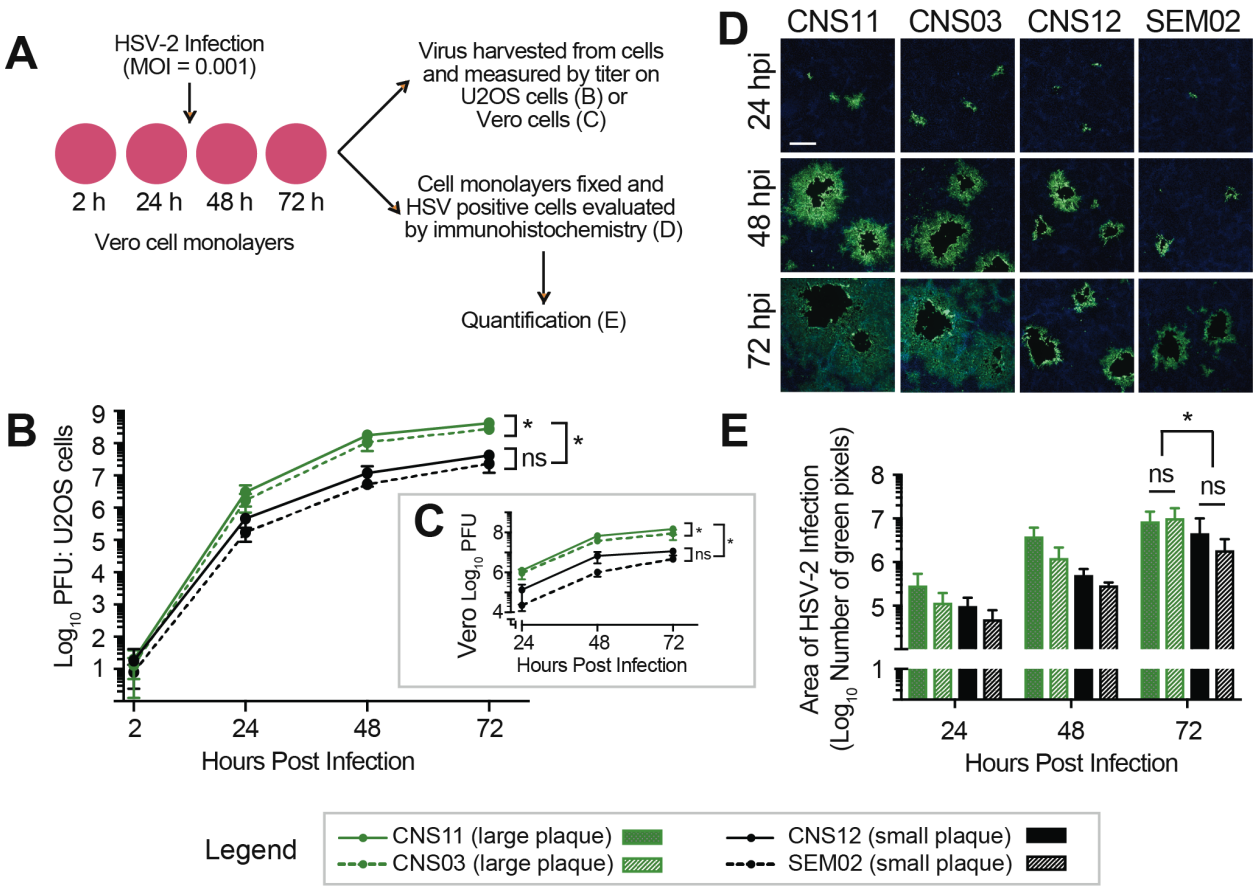

Figure 3. Enhanced viral cell-to-cell spread contributes to increased plaque size in culture.

(**A**) The rate of viral spread in Vero cells was compared for representative neonatal isolates, including large-plaque-formers (green) and small-plaque-formers (black). Vero cell monolayers were infected at MOI=0.001 in the presence of 0.1% human serum, which was replenished every 24 h. Samples were harvested at each time point and viral titer was evaluated by plaque formation on U2OS cells **(B)** or Vero cells **(C).** These data represent three independent experiments. Two-way ANOVA followed by Tukey's multiple comparison test, *p<0.0001 at 72 h. **(D)** In parallel experiments, HSV positive cells (green) were evaluated by immunofluorescence. Cell nuclei are counterstained with DAPI (blue). Scale bar = 200 μm. Images are representative of three independent experiments. Images of the entire 10 mm coverslips were then captured and stitched to create a composite image (see **Figure S2**). (**E**) The total number of immunofluorescent (green) pixels was quantified for each coverslip. Two-way ANOVA followed by Tukey's multiple comparison test, *p<0.05 at 72 h.

943

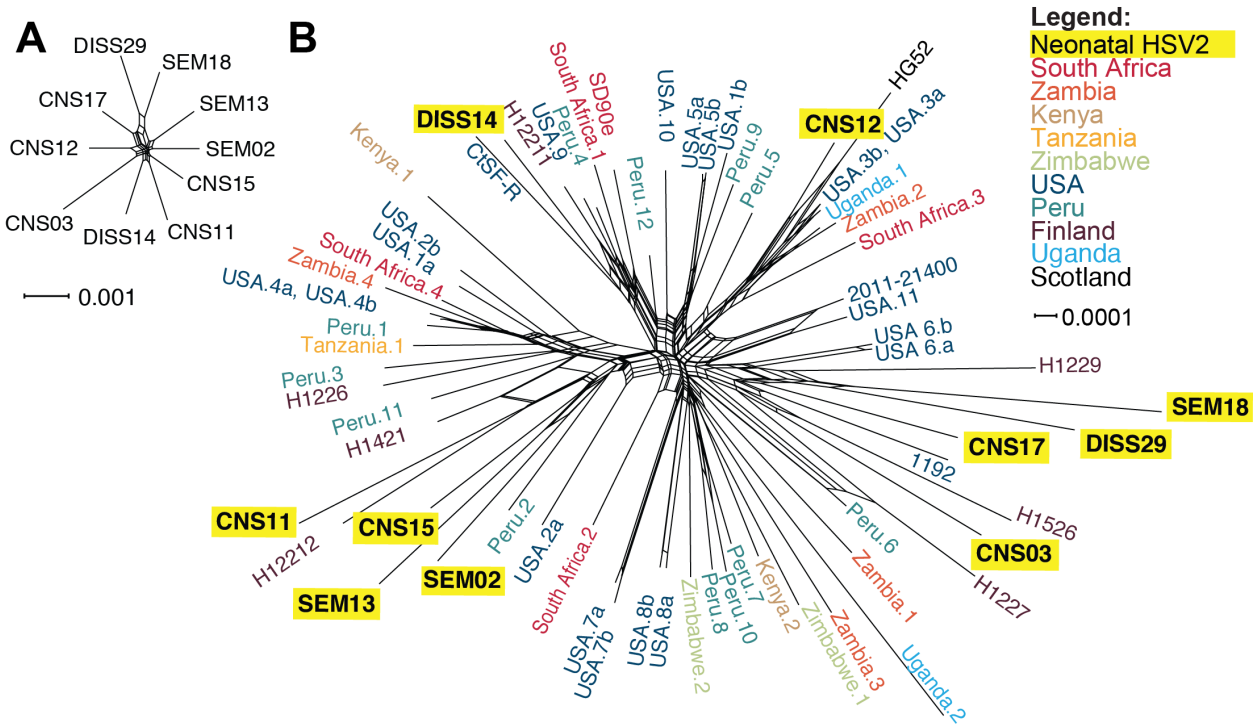

944

945 **Figure 4. Neonatal HSV-2 genomes are genetically distinct from one another and**

946 **encompass a broad range of known HSV-2 genetic diversity.**

947 A phylogenetic network constructed among neonatal HSV-2 genomes (**A**), or neonatal and adult

948 HSV-2 genomes (**B**), reveals the wide genetic distribution of these unrelated isolates. HSV-2

949 genomes have been previously noted to lack geographic separation into clades (41, 42, 82). The

950 network was created using SplitsTree4, from a MAFFT trimmed genome alignment. See **Figure**

951 **S3** for a comparison tree constructed using a neighbor-joining (NJ) algorithm. See **Table S1** for a

952 complete list of accessions, geographic origins, and references for all 58 adult HSV2 strains.

953

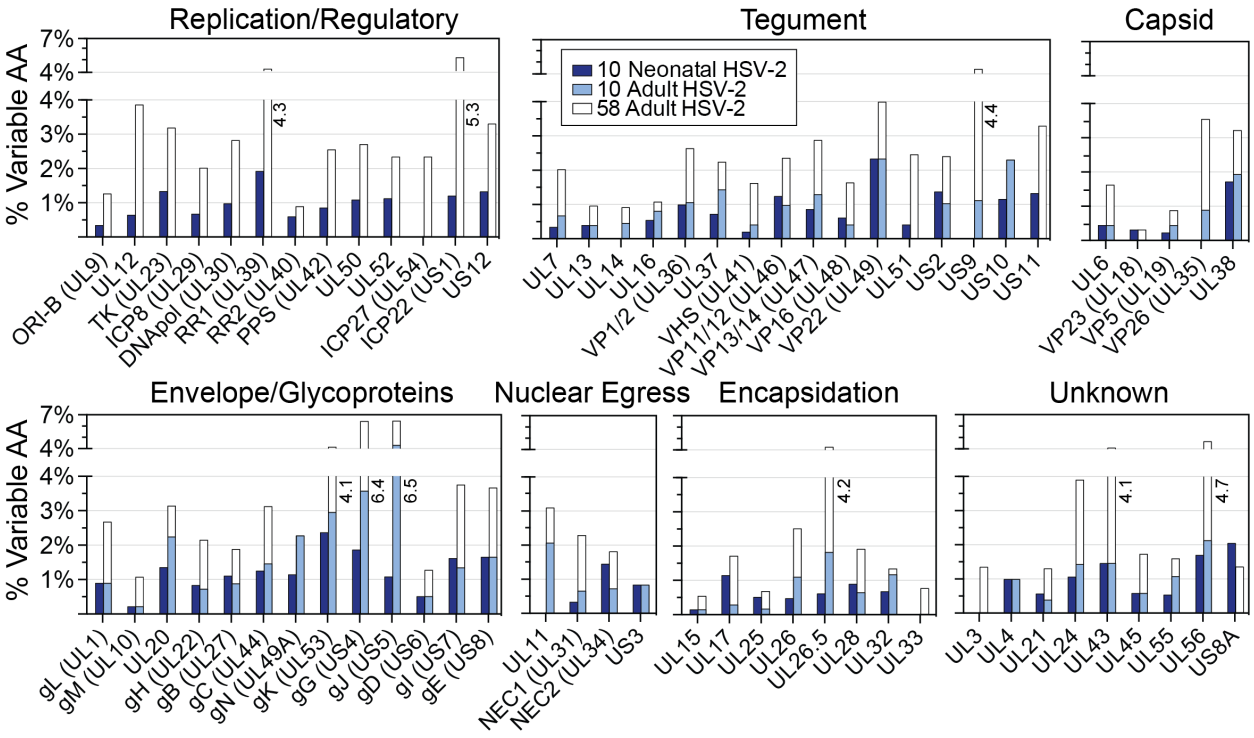

954

955 **Figure 5: Neonatal HSV-2 proteins contain a similar degree of consensus-level**

956 **amino acid (AA) differences as adult HSV-2 isolates.**

957 HSV-2 proteins are grouped by function, and the percentage of variable AAs in each protein

958 (#AA differences divided by protein length) are plotted for the 10 neonatal isolates (dark blue),

959 for 10 representative adult HSV-2 isolates (light blue), and for all 58 annotated adult HSV-2

960 genomes in GenBank (clear outlines behind light blue boxes). All adult HSV-2 genomes used for

961 this comparison are listed in **Table S1**.

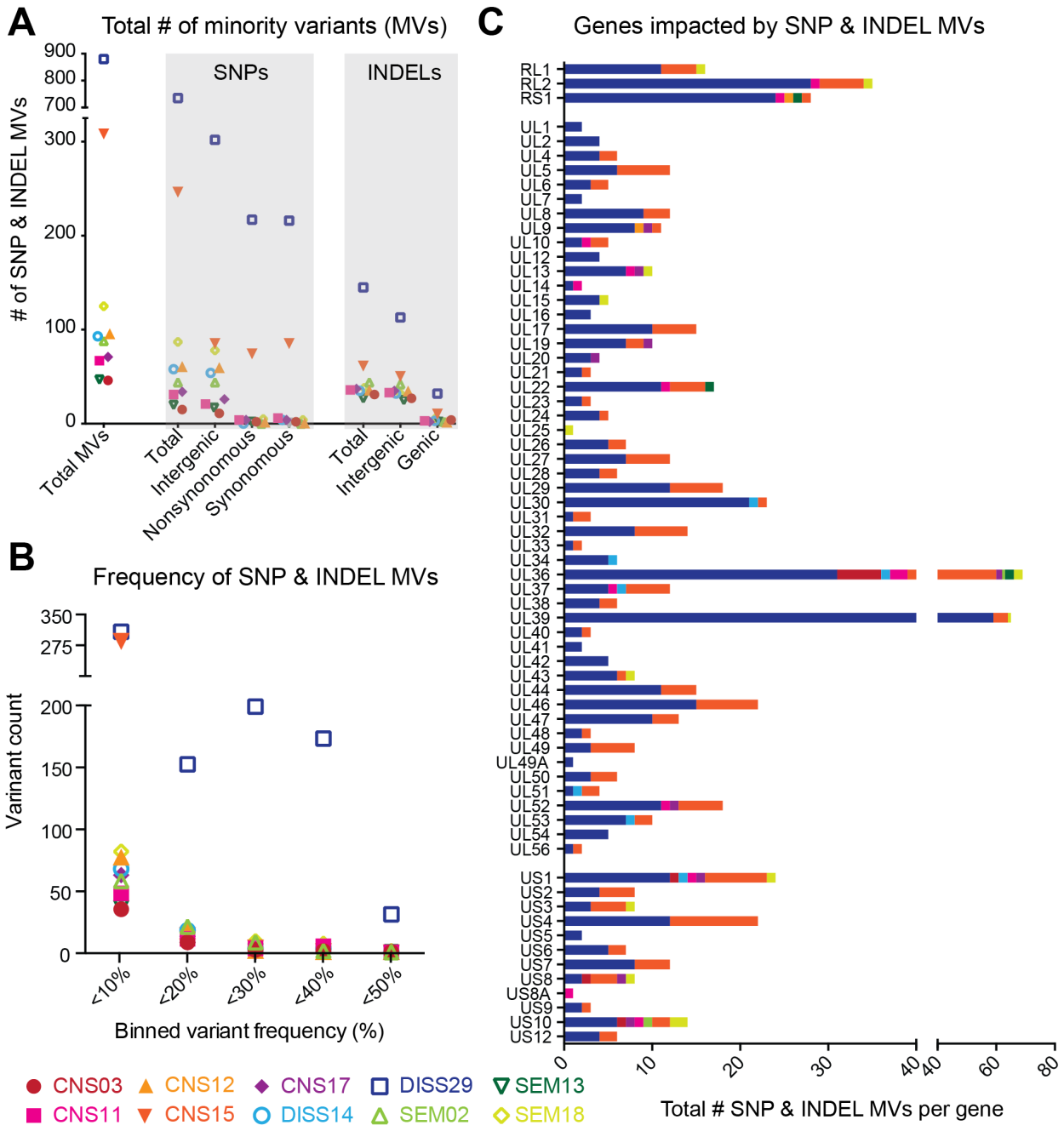

Figure 6: Minority variants expand the range of neonatal HSV-2 coding diversity.

(**A**) Scatter plot indicates the total number of minor variants (MV; y-axis) observed in each neonatal isolate. MV are rare alleles that exist within each viral population, below the level of the consensus genome. The total number of MV on the left is separated into single-nucleotide

967 polymorphism (SNP) vs. insertion/deletion (INDEL) variants on the right (x-axis). The genomic
968 location of each SNP or INDEL variant is also summarized: intergenic vs. inside of genes (genic)
969 for INDELS, and intergenic vs. nonsynonymous or synonymous SNPs inside of genes. (**B**) The
970 frequency, or penetrance, of each minority variant was examined for each isolate. Data (x-axis)
971 was binned in increments of 5% (e.g. 0-<5% frequency, 5-<10% frequency, and so on), and
972 plotted according to the number of MV observed at each frequency (y-axis). SNP and INDEL
973 variants were combined for this analysis. (**C**) Stacked histograms show the number of genic MV
974 (x-axis) located in each HSV-2 coding sequence (gene; y-axis). SNP and INDEL variants were
975 combined for this analysis. UL3, UL11, UL35, and UL55 lacked any minority variants and are
976 not included in the histogram. See **Table S3** for full list of SNP and INDEL MV position and
977 frequency data.

978

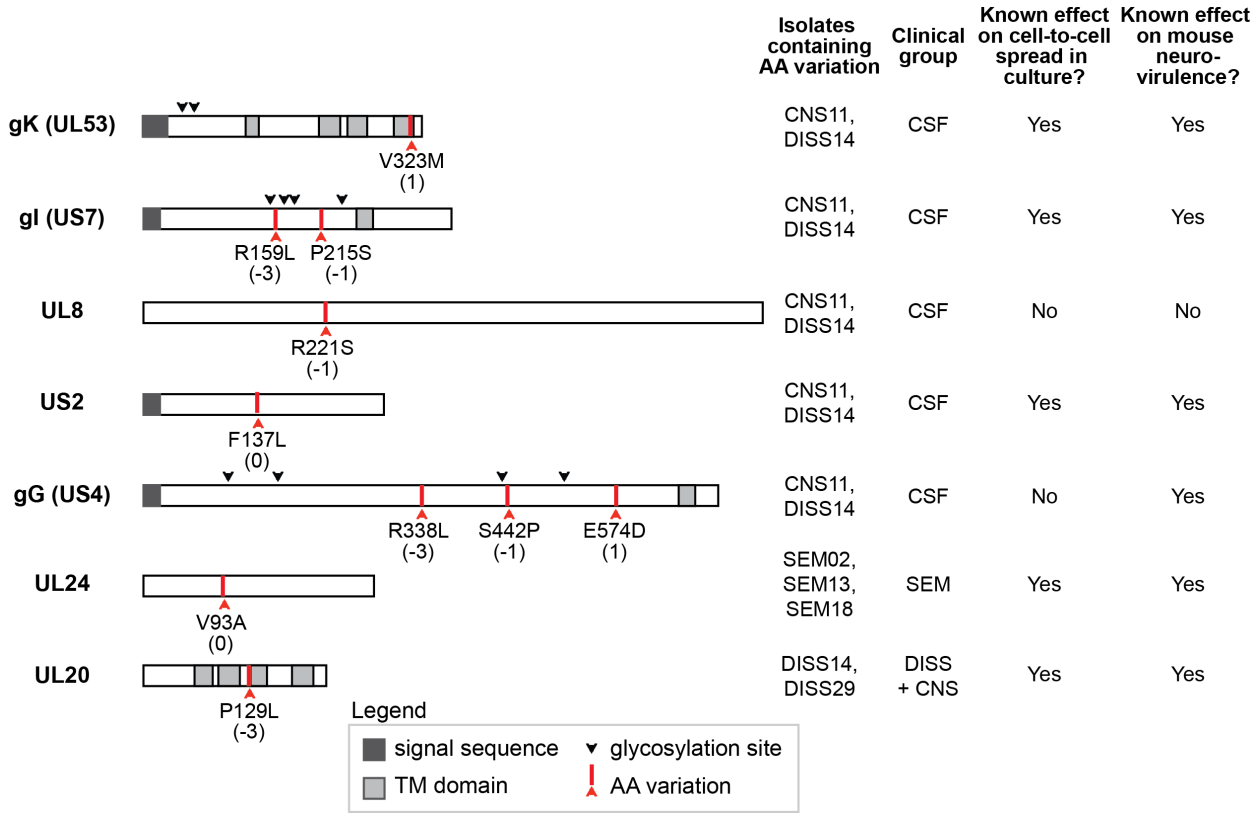

979

980 **Figure 7. Coding variations identified in neonatal HSV-2 isolates in proteins known**

981 **to contribute to cell-to-cell spread and neurovirulence.**

982 The domain structure of each HSV protein is based on published literature for both HSV-1 and -

983 2. Red arrows indicate protein-coding variations discussed in the text, with the BLOSUM80

984 score for each AA substitution listed in parenthesis beneath the highlighted difference. More

985 detailed information regarding cell-to-cell spread and neurovirulence can be found in **Table S4**.

986

Supplementary Information for

Genotypic and phenotypic diversity within the neonatal HSV-2 population

Lisa N. Akhtar, Christopher D. Bowen, Daniel W. Renner, Utsav Pandey[2], Ashley N. Della Fera, David W. Kimberlin, Mark N. Prichard, Richard J. Whitley, Matthew D. Weitzman*, Moriah L. Szpara*

***Co-Corresponding Authors**
Moriah L. Szpara
Email: moriah@psu.edu

Matthew D. Weitzman
Email: weitzmanm@email.chop.edu

This file includes:
- Supplementary Text
- Figs. S1 to S5
- Tables S1, S2 and S4
- References for SI reference citations

Other supplementary materials for this manuscript include the following:
- Table S3 in separate Excel file (two sheets, listing minority variant SNPs and INDELs)

Supplementary Text

Virus source

Viruses analyzed were collected from neonates that were culture- or PCR-confirmed to have HSV-2 infection, enrolled in three published clinical studies (1–3) by the Collaborative Antiviral Study Group (CASG) at the University of Alabama Birmingham (UAB). These HSV isolates

1016 originated from patients with SEM, CNS, or disseminated (DISS) disease with CNS involvement
1017 (**Table 1**). Samples were collected at the time of diagnosis, prior to initiation of acyclovir
1018 therapy, from either the cerebrospinal fluid (CSF) or skin. Viral isolates are associated with de-
1019 identified clinical information including age, sex, race, and clinical morbidity scores, as
1020 approved by the UAB Institutional Review Board (IRB). Enrollment in the original studies was
1021 evenly split between males and females, and included both black and white patients. Clinical
1022 morbidity score was determined by the CASG after 12 months of life as (1) normal; (2) mild
1023 impairment which includes ocular sequelae (keratoconjunctivitis), speech delay, or mild motor
1024 delay; (3) moderate impairment which includes hemiparesis, persistent seizure disorder, or
1025 developmental delay of less than or equal to 3 months adjusted developmental age; (4) severe
1026 impairment which includes microcephaly, spastic quadriplegia, chorioretinitis or blindness, or a
1027 serious developmental delay of least 3 months according to the Denver Developmental
1028 Assessment Scale (4, 5). These assessments were performed at each collaborating site. Initial
1029 collection of samples was approved by the UAB IRB. Use of these samples in this study was
1030 approved by the UAB IRB.

1031 **Cell culture**

1032 Human lung fibroblast MRC-5 cells (ATCC®, CCL-171) were cultured in minimum essential
1033 medium Eagle (MEME, Sigma-Aldrich; M5650) supplemented with 10% fetal bovine serum
1034 (FBS, Hyclone; SH30071.03), 2mM L-glutamine (Gibco, A2916801) and 1X penicillin-
1035 streptomycin (Gibco; 15140122). African green monkey kidney Vero cells (ATCC®, CCL-81)
1036 and human epithelial bone osteosarcoma U2OS cells (ATCC®, HTB-96) were cultured in
1037 Dulbecco's modified Eagle's medium with high glucose (DMEM, Hyclone; SH30081.02)

1038 supplemented with 10% FBS, 2mM L-glutamine, and 1X penicillin-streptomycin. Cell lines
1039 were authenticated by ATCC prior to purchase, and were confirmed to be mycoplasma free
1040 throughout experiments by periodic testing (LookOut Mycoplasma, Sigma).

1041 **Virus culture**

1042 Initial viral isolates (passage 1-2) were obtained from CASG samples stored at the UAB. Each
1043 isolate had been cultured at the time of diagnosis, aliquoted after one passage, and snap frozen.
1044 To conduct viral genome sequencing and phenotypic assays, each stock was expanded over three
1045 serial passages by infecting monolayers of human MRC-5 cells at a MOI of 0.01. Each infection
1046 was allowed to progress to complete cytopathic effect (CPE) before harvest (between 50-70
1047 hours), with increasing cell volume at each passage to produce sufficient virions for subsequent
1048 phenotypic and genomic comparisons. Viral stocks were titered on monolayers of either Vero
1049 cells or U2OS cells, for 100 or 48 hours respectively, to allow plaques to develop. Plaque
1050 formation was facilitated by limiting viral diffusion with a methylcellulose overlay. Plaque size
1051 and morphology were monitored carefully and did not change for any viral isolates over the
1052 course of virus stock expansion.

1053 **Plaque measurements**

1054 After appropriate incubation plaques were stained with 0.5% methylene blue and allowed to dry.
1055 Serial 4X brightfield images were collected on an EVOS FL Auto Imaging System and stitched
1056 by EVOS software to create an image of the entire well (University of Pennsylvania Cell and
1057 Developmental Biology Microscopy Core). No processing was performed. The area of 100
1058 plaques was measured for each viral isolate using ImageJ software.

1059 **Genome copy number estimation by quantitative PCR for UL27**

1060 DNA was extracted using a PureLink genomic DNA mini kit (ThermoFisher Scientific). Viral
1061 genome copy number was determined using an established assay based on real-time PCR using
1062 primers and dual-fluorescent probe specific to viral glycoprotein B gene (gB; UL27) . Samples
1063 were assayed alongside a standard curve of HSV-1 strain F nucleocapsid DNA (6), on a ViiA 7
1064 Real-Time PCR System.

1065 **Viral entry assay**

1066 Monolayers of Vero cells were cooled to 4°C for 30 minutes prior to infection and 100 PFU of
1067 each viral isolate was applied to cell monolayers at 4°C for 1 hour to allow virus binding, after
1068 which unbound virus was washed from the cells. Cells were then moved to 37°C to allow virus
1069 entry. At 0, 10, 20, 30, 45, or 60 minutes, a low-pH citrate buffer was applied to infected cells to
1070 inactivate virus that had not penetrated the cellular membrane. At each time point and for each
1071 virus, parallel infections were performed without the addition of citrate solution. These served as
1072 controls to determine the maximum number of plaques formed. Cell monolayers were washed
1073 and overlaid with methylcellulose. Plaques were scored after 100 hours of incubation. Viral entry
1074 was quantified as the fraction of plaques formed following citrate buffer application, where
1075 100% is the number of plaques formed on a monolayer not treated with citrate buffer (control).

1076 **Single-step and multi-step growth curves**

1077 Virus diluted in basic growth media containing 2% FBS was applied to near confluent
1078 monolayers of Vero cells and allowed to adsorb for 1 hour. Virus was removed and cells were
1079 incubated at 37C for the duration of infection. At 2 hpi, media containing 0.1% human serum

1080 was added to reduce the contribution of cell-free spread of virus. Single-step growth curves were
1081 performed at MOI=5 as defined by titering viral stocks on U2OS cells, and monolayers harvested
1082 at 2, 6, 12, and 24 hpi. Multi-step growth curves were performed at MOI=0.001 as defined by
1083 titering viral stocks on U2OS cells, and monolayers were harvested at 2, 24, 48, and 72 hpi.
1084 Every 24 hours, the supernatant was removed and media containing 0.1% human serum
1085 reapplied. At the conclusion of each infection, cells were washed two times with PBS and
1086 collected by scraping into an equal volume of media.

1087 **Immunocytochemistry**

1088 Multi-step growth curves were performed as described above in Vero cell monolayers grown on
1089 glass coverslips. To terminate each infection, coverslips were washed with PBS and fixed in 4%
1090 paraformaldehyde for 15 minutes at room temperature. Cells were permeabilized with 0.5%
1091 Triton-X, blocked in 3% BSA, and incubated with polyclonal rabbit antibodies raised against
1092 total HSV (Agilent Dako, B0114). After washing, cells were incubated with fluorophore-
1093 conjugated anti-Rabbit secondary antibodies (Invitrogen, A-11008) to mark HSV infected cells,
1094 and counterstained with DAPI to mark cell nuclei. Coverslips were initially visualized with a
1095 Leica DM6000 wide field microscope (UPenn Cell and Developmental Microscopy Core). The
1096 5X images were collected on a Photometrics HQ2 high resolution monochrome CCD camera,
1097 and processed with LAS AF software. The 10X images were collected on a EVOS FL Auto
1098 Imaging System (UPenn Cell and Developmental Microscopy Core) and stitched using EVOS
1099 software. Exposure and gain were optimized within each experiment for one virus at the 72-hour
1100 time point and applied identically to each image within that experiment. Any subsequent image
1101 processing (ImageJ) was applied equally to all images in a given experiment.

1102 **Immunoblotting**

1103 Whole cell lysates were prepared with 1X LDS sample buffer (NuPage) and equal amounts of
1104 lysate were separated by SDS-PAGE. Membranes were immunoblotted with polyclonal rabbit
1105 antibodies raised against total HSV (Agilent Dako, B0114); glycoproteins (g)C, gD, gE, gH, and
1106 VP5 (all gifts from Gary Cohen); ICP8 (gift from David Knipe); and GAPDH (GeneTex,
1107 GTX100118). Proteins were visualized with Pierce ECL Western Blotting Substrate
1108 (ThermoFisher Scientific) and detected using a G:Box imaging system (Syngene).

1109 ***De novo* genome assembly**

1110 A consensus genome was assembled for each viral isolate using a previously described Viral
1111 Genome Assembly (VirGA) bioinformatics workflow (7). VirGA begins by quality-filtering the
1112 MiSeq sequence reads and removing sequences that match the host (human) genome. Thereafter
1113 VirGA uses a combination of SSAKE *de novo* assemblies run with differing parameters, which
1114 are then combined into a single draft genome using Celera and GapFiller (8–10). After quality-
1115 checking and iterative improvement of the genome assembly, annotations were transferred from
1116 the HSV-2 reference genome (strain HG52; GenBank NC_001798) to each new genome based
1117 on sequence homology (11).

1118 **Comparative genomics and phylogenetic analysis**

1119 The genomes of all 10 neonatal HSV-2 isolates were combined with all annotated HSV-2
1120 genomes available in GenBank (see **Table S1** for full list) and aligned using MAFFT (12). All
1121 previously published HSV-2 genomes were derived from infected adults. The genome-wide
1122 alignment used a trimmed genome format (lacking the terminal repeats) to avoid giving undue

1123 weight to these duplicated sequences. The MAFFT alignment was used to generate a
1124 NeighborNet phylogenetic network in SplitsTree with Uncorrected P distances (13–15). A
1125 diverse subset of ten adult HSV-2 isolates was selected for protein-level comparisons with the
1126 ten neonatal isolates; these are indicated in **Table S1** with an asterisk. GenBank genomes that
1127 lacked open reading frame (ORF) and protein annotations were excluded from all comparisons
1128 (16, 17). ClustalW2 was used to construct pairwise nucleotide alignments between whole
1129 genomes and pairwise amino acid alignments for each gene and protein (18). Pan-HSV2
1130 comparisons excluded three viral proteins for which sequences are not fully determined in most
1131 published strains, likely due to the high G+C-content and numerous tandem repeats in these
1132 regions: ICP34.5 (RL1 – annotated/complete in only 9 genomes from **Table S1**), ICP0 (RL2 –
1133 annotated/complete in only 8 genomes from **Table S1**), and ICP4 (RS1 – annotated/complete in
1134 only 6 genomes from **Table S1**) (16, 19, 20). Alignments for RL1, RL2, and RS1 for neonatal
1135 isolates were hand-curated to optimize alignment and translation around sequencing gaps, to
1136 avoid over-representing the degree of divergence in these three genes.

1137

1138 # Supporting Figures & Tables

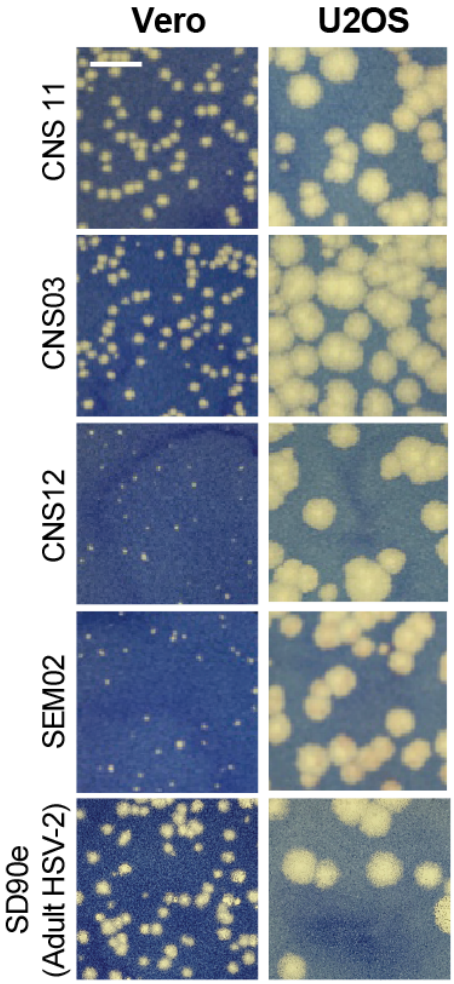

1139

1140 **Figure S1. U2OS cells support large plaque formation by all isolates.**

1141 Representative plaques are shown after neonatal viruses were allowed to incubate for 100 hours

1142 on Vero **(A)** or U2OS cells **(B)**. All neonatal isolates were capable of forming large plaques on

1143 U2OS cells, which lack innate sensing of viral infection through the STING pathway (21).

1144

1145

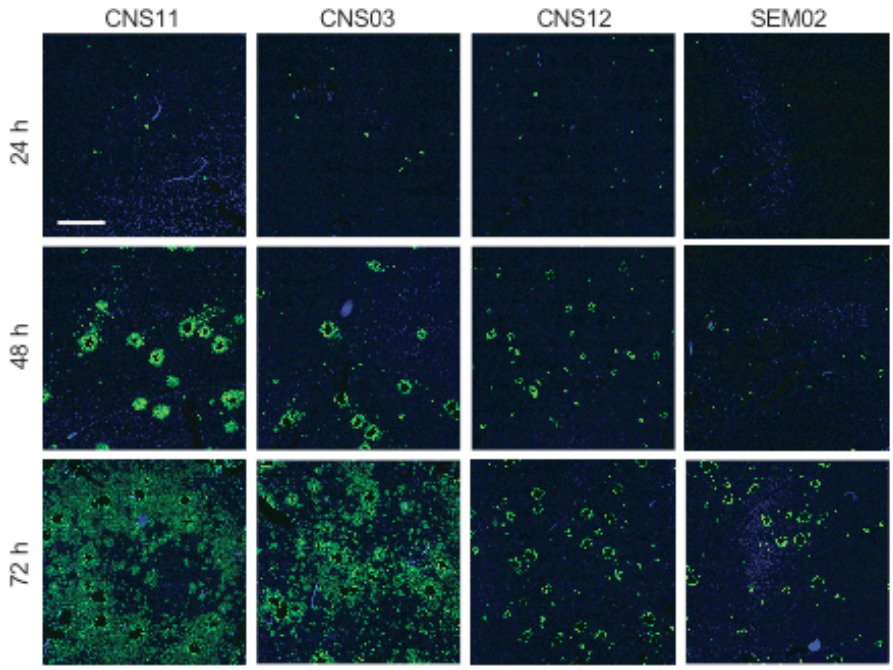

1146

1147 **Figure S2. Cell-to-cell spread is enhanced in certain neonatal HSV-2 isolates.**

1148 Confluent Vero cell monolayers were infected at MOI=0.001 for the time points indicated, in the
1149 presence of 0.1% human serum. HSV positive cells (green) were evaluated at each time point by
1150 immunofluorescence. Cell nuclei are counterstained with DAPI (blue). Serial 10X images were
1151 obtained on an EVOS FL Auto Imaging System and stitched together to create an image of the
1152 entire experimental coverslip. Scale bar = 1mm. These images were quantified in **Figure 3E**.

1153

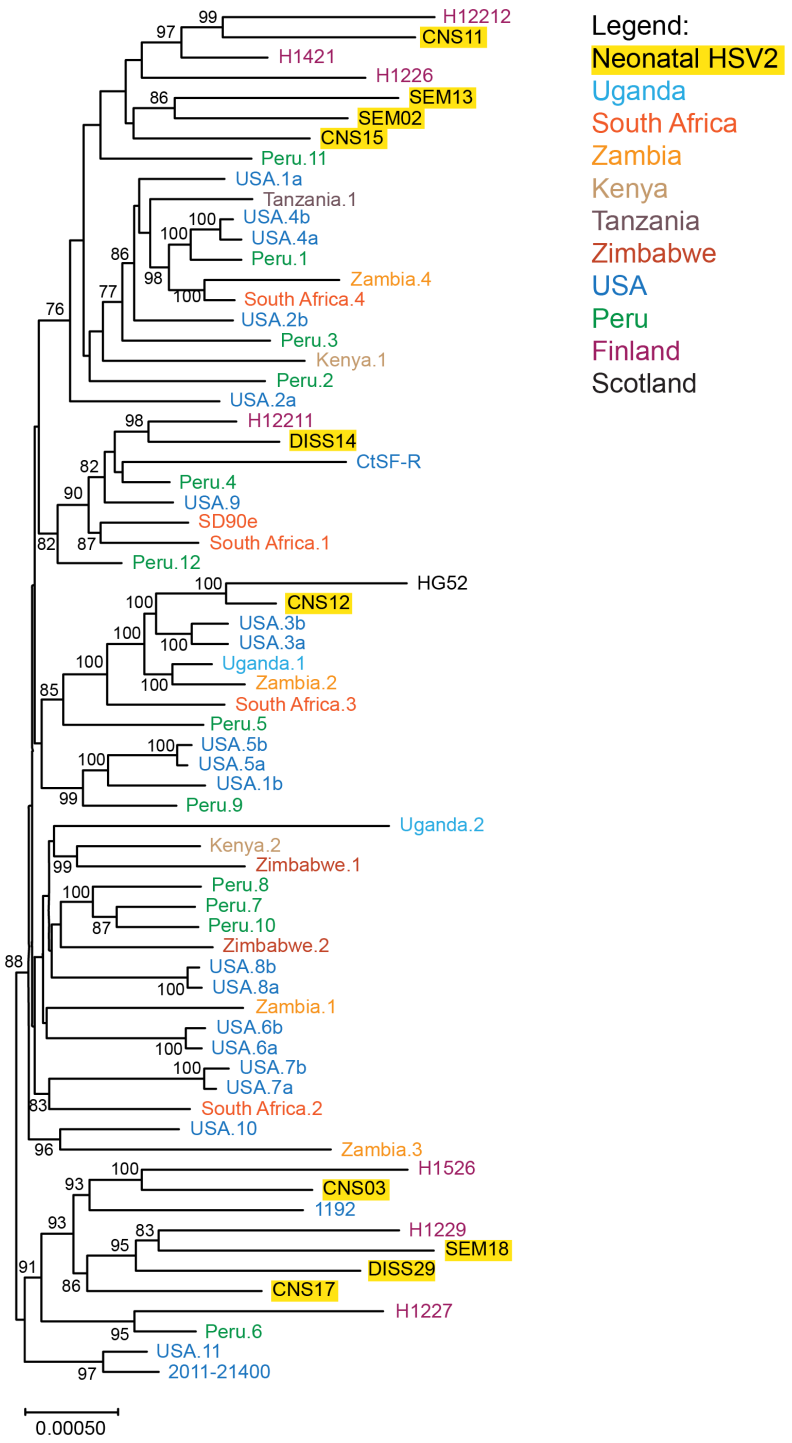

Figure S3. Phylogenetic clustering demonstrates that neonatal HSV-2 genomes are genetically distinct from one another and intermingle with the previously known range of HSV-2 genetic diversity.

1158 A Neighbor-Joining (NJ) tree network constructed among ten neonatal and 58 adult HSV-2
1159 genomes, revealed the wide genetic distribution of the neonatal isolates. The NJ tree (Jukes-
1160 Cantor, 1000 bootstraps) was created in MEGA from a MAFFT trimmed genome alignment.
1161 Bootstrap values $\geq$ 70 are shown here. See **Figure 4** for a network graph comparison to this tree.
1162 **Table S1** contains a complete list of accessions, geographic origins, and references for all adult
1163 HSV2 strains.

1164

1165

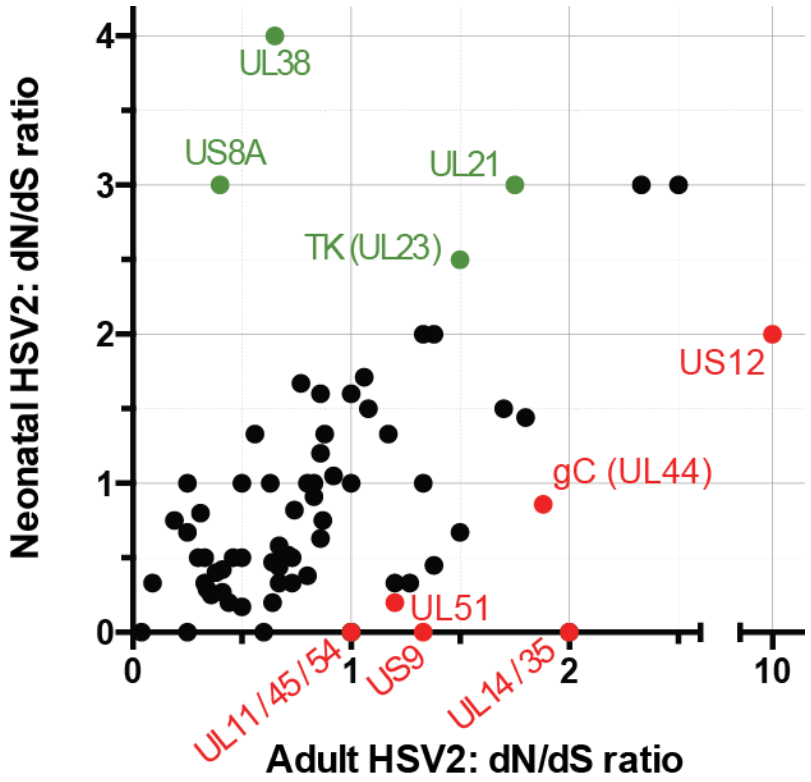

1166

1167 **Figure S4. Ratio of non-synonymous to synonymous coding variations in neonatal**

1168 **HSV-2 versus adult HSV-2 strains.**

1169 The ratio of non-synonymous (dN) to synonymous (dS) coding variations were plotted for each

1170 HSV-2 protein. The x-axis value represents the average dN/dS ratio for each protein in 58 adult

1171 HSV-2 strains, while the y-axis value represents the average dN/dS ratio in 10 neonatal isolates.

1172 Proteins with a difference in average dN/dS ratios ≥1 in neonatal vs. adult HSV-2 genomes are

1173 labeled (green indicates a higher average dN/dS in neonatal HSV-2 genomes; red indicates a

1174 higher dN/dS in adult HSV-2 genomes). The average dN/dS ratios for all proteins are listed in

1175 **Table S2**.

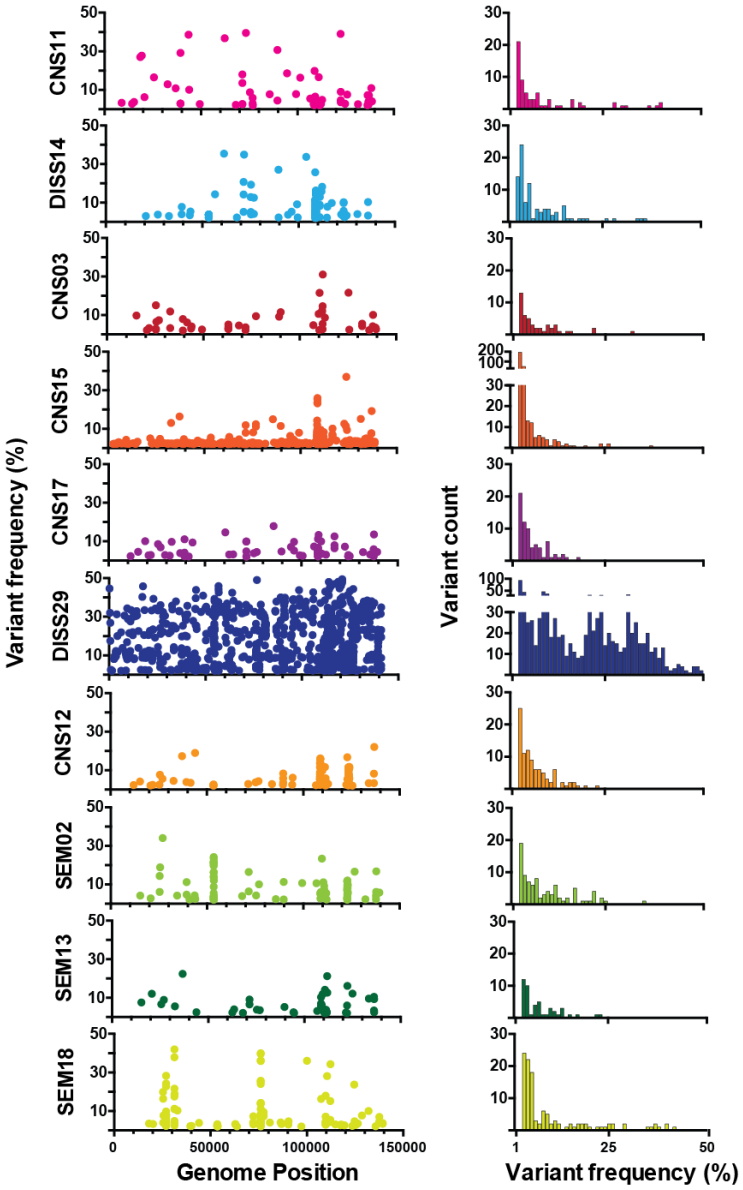

Figure S5. Genome-wide distribution and frequency of minority variants in neonatal HSV-2 isolates.

For each neonatal HSV-2 isolate, the graph on the left plots spatial location in the genome (x-axis) against the frequency at which each minority variant was observed. The plot on the right summarizes the number of minor variants (y-axis height) in binned increments of 1% (x-axis). The data reveal the distinctly different distribution of minority variants in DISS29, and to a lesser extent CNS15, than in other isolates. Color code matches that used in **Figure 6**. See **Table S3** for full list of SNP and INDEL MV position and frequency data.

1185 **Table S1. Adult HSV-2 genomes (58 total) used for comparative genomic analyses.**

Virus Isolate	Country (with location, if available)	GenBank Accession #	References
H1227*	Finland	KY922721	In process
H1229*	Finland	KY922722	In process
H12212*	Finland	KY922726	In process
Uganda.2*	Uganda	KX574906	(20)
Peru.8*	Peru	KX574874	(20)
Zambia.4*	Zambia	KX574883	(20)
HG52*	Scotland	NC_001798	(22)
CtSF-R*	USA	KP334093	(19)
1192*	Wisconsin, USA	KP334095	(19)
SD90e*	Carletonville, South Africa	KF781518	(23, 24)
Peru.1	Peru	KX574860	(20, 25)
Peru.12	Peru	KX574861	(20, 25)
Zambia.3	Zambia	KX574862	(20, 25)
Zimbabwe.2	Zimbabwe	KX574863	(20, 25)
Zambia.2	Zambia	KX574864	(20, 25)
Peru.9	Peru	KX574865	(20, 25)
Peru.11	Peru	KX574866	(20, 25)
Peru.10	Peru	KX574867	(20, 25)
USA.8a	USA	KX574868	(20, 25)
USA.8b	USA	KX574869	(20, 25)
USA.1b	USA	KX574870	(20, 25)
Zimbabwe.1	Zimbabwe	KX574871	(20, 25)
Peru.7	Peru	KX574872	(20, 25)
Peru.2	Peru	KX574873	(20, 25)
Peru.6	Peru	KX574875	(20, 25)
Peru.4	Peru	KX574876	(20, 25)
Peru.3	Peru	KX574877	(20, 25)
Peru.5	Peru	KX574878	(20, 25)
South Africa.2	South Africa	KX574879	(20, 25)
South Africa.3	South Africa	KX574880	(20, 25)
South Africa.4	South Africa	KX574881	(20, 25)
USA.3a	USA	KX574882	(20, 25)
USA.3b	USA	KX574884	(20, 25)
USA.2b	USA	KX574885	(20, 25)
USA.10	USA	KX574886	(20, 25)
USA.4a	USA	KX574887	(20, 25)
USA.7a	USA	KX574888	(20, 25)
USA.6a	USA	KX574889	(20, 25)

Virus Isolate	**Country (with location, if available)**	**GenBank Accession #**	**References**
USA.6b	USA	KX574890	(20, 25)
USA.5a	USA	KX574891	(20, 25)
South Africa.1	South Africa	KX574892	(20, 25)
Kenya.2	Kenya	KX574893	(20, 25)
Kenya.1	Kenya	KX574894	(20, 25)
USA.7b	USA	KX574895	(20, 25)
USA.5b	USA	KX574896	(20, 25)
USA.11	USA	KX574897	(20, 25)
USA.4b	USA	KX574898	(20, 25)
Uganda.1	Uganda	KX574899	(20, 25)
USA.9	USA	KX574901	(20, 25)
Tanzania.1	Tanzania	KX574902	(20, 25)
USA.1a	USA	KX574903	(20, 25)
USA.2a	USA	KX574904	(20, 25)
Zambia.1	Zambia	KX574905	(20, 25)
2011-21400	USA	KX574908	(20, 25)
H12211	Finland	KY922725	In process
H1226	Finland	KY922720	In process
H1421	Finland	KY922723	In process
H1526	Finland	KY922724	In process

*Indicates 10 adult HSV2 strains used for AA comparisons in Figure 5.

Table S2. Number of nucleotide and amino acid (AA) differences observed in each set of neonatal or adult HSV2 genomes.

Gene*	ORF length in NT^	protein length (#AA)	10 Neonatal # NT diff.^	10 Neonatal # AA changes	10 Neonatal %AA diff.	10 Neonatal dN/dS ratio	10 Adult # NT diff.	10 Adult # AA changes	10 Adult %AA diff.	10 Adult dN/dS ratio	58 Adult # NT diff.	58 Adult # AA diff.	58 Adult %AA diff.	58 Adult dN/dS ratio
UL1	675	225	5	2	0.9	0.7	3	2	0.9	2.0	10	6	2.7	1.5
UL2	1,005	335	7	4	1.2	1.3	10	3	0.9	0.4	14	5	1.5	0.6
UL3	669	223	1	0	0.0	0.0	2	0	0.0	0.0	8	3	1.3	0.6
UL4	606	202	5	2	1.0	0.7	6	2	1.0	0.5	10	2	1.0	0.3
UL5	2,646	882	18	4	0.5	0.3	21	3	0.3	0.2	43	11	1.2	0.3
UL6	2,037	679	9	3	0.4	0.5	6	3	0.4	1.0	26	11	1.6	0.7
UL7	891	297	4	1	0.3	0.3	5	2	0.7	0.7	15	6	2.0	0.7
UL8	2,259	753	13	5	0.7	0.6	18	7	0.9	0.6	39	18	2.4	0.9
UL9	2,616	872	9	3	0.3	0.5	14	4	0.5	0.4	35	11	1.3	0.5
UL10	1,404	468	5	1	0.2	0.3	6	1	0.2	0.2	19	5	1.1	0.4
UL11	291	97	1	0	0.0	0.0	4	2	2.1	1.0	6	3	3.1	1.0
UL12	1,863	621	6	4	0.6	2.0	14	9	1.4	1.8	42	24	3.9	1.3
UL13	1,557	519	8	2	0.4	0.3	6	2	0.4	0.5	20	5	1.0	0.3
UL14	660	220	3	0	0.0	0.0	2	1	0.5	1.0	3	2	0.9	2.0
UL15	2,205	735	2	1	0.1	1.0	4	1	0.1	0.3	20	4	0.5	0.3
UL16	1,119	373	4	2	0.5	1.0	5	3	0.8	1.5	8	4	1.1	1.0
UL17	2,109	703	13	8	1.1	1.6	9	2	0.3	0.3	24	12	1.7	1.0
UL18	957	319	4	1	0.3	0.3	4	0	0.0	0.0	12	1	0.3	0.1
UL19	4,125	1,375	14	3	0.2	0.3	21	6	0.4	0.4	41	12	0.9	0.4
UL20	669	223	4	3	1.3	3.0	6	5	2.2	5.0	10	7	3.1	2.3
UL21	1,599	533	4	3	0.6	3.0	3	2	0.4	2.0	11	7	1.3	1.8
UL22	2,517	839	22	7	0.8	0.5	20	6	0.7	0.4	46	18	2.1	0.6
UL23	1,131	377	7	5	1.3	2.5	11	6	1.6	1.2	20	12	3.2	1.5
UL24	846	282	12	3	1.1	0.3	14	4	1.4	0.4	26	11	3.9	0.7
UL25	1,758	586	7	3	0.5	0.8	8	1	0.2	0.1	25	4	0.7	0.2
UL26	1,914	638	11	3	0.5	0.4	18	7	1.1	0.6	36	16	2.5	0.8
UL26.5	990	330	8	2	0.6	0.3	11	6	1.8	1.2	25	14	4.2	1.3

Gene*	ORF length in NT^	protein length (#AA)	10 Neonatal # NT diff.^	10 Neonatal # AA changes	10 Neonatal %AA diff.	10 Neonatal dN/dS ratio	10 Adult # NT diff.	10 Adult # AA changes	10 Adult %AA diff.	10 Adult dN/dS ratio	58 Adult # NT diff.	58 Adult # AA diff.	58 Adult %AA diff.	58 Adult dN/dS ratio
UL27	2,715	905	16	10	1.1	1.7	17	8	0.9	0.9	39	17	1.9	0.8
UL28	2,358	786	14	7	0.9	1.0	11	5	0.6	0.8	39	15	1.9	0.6
UL29	3,591	1,197	27	8	0.7	0.4	32	11	0.9	0.5	83	24	2.0	0.4
UL30	3,723	1,241	19	12	1.0	1.7	39	20	1.6	1.1	68	35	2.8	1.1
UL31	918	306	6	1	0.3	0.2	9	2	0.7	0.3	18	7	2.3	0.6
UL32	1,797	599	13	4	0.7	0.4	13	7	1.2	1.2	20	8	1.3	0.7
UL33	393	131	2	0	0.0	0.0	1	0	0.0	0.0	5	1	0.8	0.3
UL34	831	277	8	4	1.4	1.0	7	2	0.7	0.4	15	5	1.8	0.5
UL35	339	113	0	0	0.0	0.0	2	1	0.9	0.0	6	4	3.5	2.0
UL36	9,369	3,123	65	31	1.0	0.9	73	33	1.1	0.8	181	82	2.6	0.8
UL37	3,345	1,115	13	8	0.7	1.6	27	16	1.4	1.5	54	25	2.2	0.9
UL38	1,401	467	10	8	1.7	4.0	22	9	1.9	0.7	38	15	3.2	0.7
UL39	3,429	1,143	64	22	1.9	0.5	72	25	2.2	0.5	118	49	4.3	0.7
UL40	1,014	338	6	2	0.6	0.5	4	0	0.0	0.0	13	3	0.9	0.3
UL41	1,479	493	6	1	0.2	0.2	13	2	0.4	0.2	26	8	1.6	0.4
UL42	1,413	471	8	4	0.8	1.0	16	8	1.7	1.0	21	12	2.5	1.3
UL43	1,245	415	10	6	1.4	1.5	8	6	1.4	3.0	27	17	4.1	1.7
UL44	1,443	481	13	6	1.2	0.9	12	7	1.5	1.4	23	15	3.1	1.9
UL45	519	173	1	1	0.6	0.0	3	1	0.6	0.0	6	3	1.7	1.0
UL46	2,169	723	20	9	1.2	0.8	18	7	1.0	0.6	40	17	2.4	0.7
UL47	2,091	697	14	6	0.9	0.8	13	9	1.3	2.3	43	20	2.9	0.9
UL48	1,473	491	6	3	0.6	1.0	7	2	0.4	0.4	18	8	1.6	0.8
UL49	903	301	19	7	2.3	0.6	17	7	2.3	0.7	30	12	4.0	0.7
UL49A	264	88	3	1	1.1	0.5	6	2	2.3	0.5	8	2	2.3	0.3
UL50	1,110	370	8	4	1.1	1.0	7	4	1.1	1.3	22	10	2.7	0.8
UL51	735	245	6	1	0.4	0.2	1	0	0.0	0.0	11	6	2.4	1.2
UL52	3,201	1,067	22	12	1.1	1.2	31	11	1.0	0.6	54	25	2.3	0.9
UL53	1,017	339	14	8	2.4	1.3	16	10	2.9	1.7	26	14	4.1	1.2
UL54	1,539	513	5	0	0.0	0.0	7	3	0.6	0.8	24	12	2.3	1.0
UL55	561	187	3	1	0.5	0.5	2	2	1.1	0.0	9	3	1.6	0.5
UL56	708	236	6	4	1.7	2.0	8	5	2.1	1.7	19	11	4.7	1.4

Gene*	ORF length in NT^	protein length (#AA)	10 Neonatal # NT diff.^	10 Neonatal # AA changes	10 Neonatal %AA diff.	10 Neonatal dN/dS ratio	10 Adult # NT diff.	10 Adult # AA changes	10 Adult %AA diff.	10 Adult dN/dS ratio	58 Adult # NT diff.	58 Adult # AA diff.	58 Adult %AA diff.	58 Adult dN/dS ratio
US1	1,245	415	16	5	1.2	0.5	14	6	1.4	0.8	38	22	5.3	1.4
US2	876	292	7	4	1.4	1.3	4	3	1.0	3.0	15	7	2.4	0.9
US3	1,446	482	9	4	0.8	0.8	7	4	0.8	1.3	17	4	0.8	0.3
US4	2,100	700	22	13	1.9	1.4	40	25	3.6	1.7	70	45	6.4	1.8
US5	279	93	4	1	1.1	0.3	8	4	4.3	1.0	11	6	6.5	1.2
US6	1,182	394	7	2	0.5	0.4	8	2	0.5	0.3	18	5	1.3	0.4
US7	1,119	373	10	6	1.6	1.5	11	5	1.3	0.8	27	14	3.8	1.1
US8	1,638	546	12	9	1.6	3.0	9	9	1.6	0.0	28	20	3.7	2.5
US8A	441	147	4	3	2.0	3.0	2	0	0.0	0.0	7	2	1.4	0.4
US9	270	90	2	0	0.0	0.0	3	1	1.1	0.5	7	4	4.4	1.3
US10	261	87	7	1	1.1	0.2	3	2	2.3	2.0	6	2	2.3	0.5
US11	456	152	2	2	1.3	0.0	0	0	0.0	0.0	136	5	3.3	0.0
US12	909	303	6	4	1.3	2.0	6	0	0.0	0.0	11	10	3.3	10.0
RL1	786	262	17	10	3.8	1.4	♦				♦			
RL2	2,502	834	40	20	2.4	1.0	♦				♦			
RS1	3957	1319	42	26	2.0	1.6	♦				♦			

* See **Table S1** for list of strain names and genome accessions for comparisons of 10 neonatal, 10 adult, and 58 adult HSV2 genomes.

♦ Less than 10 strains from Table S1 have complete sequences of these genes; see Methods for details.

^ Abbreviations: ORF, open reading frame; NT, nucleotide; AA, amino acid; diff., difference; %, percent; dN/dS, ratio of nonsynonymous to synonymous nucleotide changes

Table S4. Viral genetic variations potentially associated with clinical groups.

HSV-2 Gene: Variation	Clinical Group (Isolates w/ Variation)	Predicted effect^	Protein Function	Neurovirulence
gK (UL53): V323M	All CSF Isolates (CNS11, DISS14)	Loss of one TM domain	Glycoprotein at virion and cell surface; interacts with gB and UL20 (26); important for cytoplasmic envelopment, viral egress, and virus-induced cell fusion	gK null virus exhibits poor neuronal spread in culture including decreased retrograde and anterograde transport (27); reduced spread within eye and to nervous system, as well as increased survival, following ocular challenge in mice (28)
gI (US7): R159L + P215S	All CSF Isolates (Both: CNS11,DISS14 R159L only: CNS03, SEM13,CNS15*,DISS29* P215S only: CNS15*,DISS29)	R159L: adds one TM domain; P215S: no change	Glycoprotein at virion and cell surface; forms heterodimer with gE to form viral Fc receptor (29); required for cell-to-cell spread of virus in epithelial and neuronal cells (30, 31);	gI null virus exhibits poor neuronal spread in culture; reduced spread in retina and to retinorecipient areas of the brain following ocular challenge in mice (31)
UL8: R221S	All CSF Isolates (CNS11, DISS14)	No predicted change	Putative primase subunit of helicase primase complex; required for unwinding of viral DNA	None identified
US2: F137L	All CSF Isolates (CNS11, DISS14)	No predicted change	Tegument protein; binds and phosphorylates TAK1 to positively regulate NFkB signaling (32)	Virus containing mutated US2 forms small plaques in culture (33); Mutant virus containing a deletion of both US2 and PK result in decreased death following intracerebral injection in mice (34)
gG (US4): R338L,S442P, E574D	All CSF Isolates (CNS11, DISS14)	No predicted change	Binds and enhances function of chemokines (35); enhances neurotrophin-dependent axonal growth in culture (36)	Virus containing mutated gG results in decreased death following intracerebral injection in mice (33)
UL24: V93A	No CNS Isolates; only found in SEM isolates (SEM02, SEM13, SEM18)	No predicted change	Membrane-associated nuclear protein; associated with dispersal of nucleolin during infection (37)	UL24 null virus forms small plaques in culture (38); decreased viral load in eye and nervous system following ocular challenge in mice **(39–41)**
UL20: P129L	All DISS Isolates w/ CNS Involved (DISS14, DISS29)	Change in position of three TM domains	Membrane-associated protein interacts with gK and gB (26); required for gK glycosylation, cell surface expression (42), and virus-induced cell fusion (43); important for viral egress (44)	UL20 null virus forms small plaques in culture (43); RNA inhibition of UL20 results in decreased rates of encephalitis following HSV footpad infection in mice (45)

* present as minority variant ^ Prediction by SMART Analysis

References

1. Kimberlin DW, Lin CY, Jacobs RF, Powell DA, Frenkel LM, Gruber WC, Rathore M, Bradley JS, Diaz PS, Kumar M, Arvin AM, Gutierrez K, Shelton M, Weiner LB, Sleasman JW, de Sierra TM, Soong SJ, Kiell J, Lakeman FD, Whitley RJ, National Institute of Allergy and Infectious Diseases Collaborative Antiviral Study Group. 2001. Natural history of neonatal herpes simplex virus infections in the acyclovir era. Pediatrics 108:223–229.

2. Kimberlin DW, Whitley RJ, Wan W, Powell DA, Storch G, Ahmed A, Palmer A, Sánchez PJ, Jacobs RF, Bradley JS. 2011. Oral acyclovir suppression and neurodevelopment after neonatal herpes. N Engl J Med 365:1284–1292.

3. Kimberlin DW, Lin CY, Jacobs RF, Powell DA, Corey L, Gruber WC, Rathore M, Bradley JS, Diaz PS, Kumar M, Arvin AM, Gutierrez K, Shelton M, Weiner LB, Sleasman JW, de Sierra TM, Weller S, Soong SJ, Kiell J, Lakeman FD, Whitley RJ, National Institute of Allergy and Infectious Diseases Collaborative Antiviral Study Group. 2001. Safety and efficacy of high-dose intravenous acyclovir in the management of neonatal herpes simplex virus infections. Pediatrics 108:230–238.

4. Whitley R, Arvin A, Prober C, Burchett S, Corey L, Powell D, Plotkin S, Starr S, Alford C, Connor J, Jacobs R, Nahmias A, Soong S-J, the National Institute of Allergy, Infectious Diseases Collaborative Antiviral Study Group*. 1991. A Controlled Trial Comparing Vidarabine with Acyclovir in Neonatal Herpes Simplex Virus Infection. N Engl J Med 324:444–449.

5. Whitley R, Arvin A, Prober C, Corey L, Burchett S, Plotkin S, Starr S, Jacobs R, Powell D, Nahmias A, Sumaya C, Edwards K, Alford C, Caddell G, Soong S-J, the National Institute of Allergy and Infectious Diseases Collaborative Antiviral Study Group*. 1991. Predictors of Morbidity and Mortality in Neonates with Herpes Simplex Virus Infections. N Engl J Med 324:450–454.

6. Szpara ML, Parsons L, Enquist LW. 2010. Sequence variability in clinical and laboratory isolates of herpes simplex virus 1 reveals new mutations. J Virol 84:5303–13.

7. Parsons LR, Tafuri YR, Shreve JT, Bowen CD, Shipley MM, Enquist LW, Szpara ML. 2015. Rapid genome assembly and comparison decode intrastrain variation in human alphaherpesviruses. mBio 6:e02213-14.

8. Myers EW, Sutton G, Delcher AL, Dew IM, Fasulo DP, Flanigan MJ, Kravitz SA, Mobarry CM, Reinert KHJ, Remington KA, Anson EL, Bolanos RA, Chou H-H, Jordan CM, Halpern AL, Lonardi S, Beasley EM, Brandon RC, Chen L, Dunn PJ, Lai Z, Liang Y, Nusskern DR, Zhan M, Zhang Q, Zheng X, Rubin GM, Adams MD, Venter CJ. 2000. A Whole-Genome Assembly of Drosophila. Science 287:2196–2204.

9. Boetzer M, Pirovano W. 2012. Toward almost closed genomes with GapFiller. Genome Biol 13:1–9.

10. Warren RL, Sutton GG, Jones SJM, Holt R a. 2007. Assembling millions of short DNA

sequences using SSAKE. Bioinformatics 23:500–1.

11. Dolan A, Jamieson FE, Cunningham C, Barnett BC, McGeoch DJ. 1998. The genome sequence of herpes simplex virus type 2. J Virol 72:2010–2021.

12. Katoh K, Misawa K, Kuma K, Miyata T. 2002. MAFFT: a novel method for rapid multiple sequence alignment based on fast Fourier transform. Nucleic Acids Res 30:3059–3066.

13. Strimmer K, Wiuf C, Moulton V. 2001. Recombination analysis using directed graphical models. Mol Biol Evol 18:97–99.

14. Norberg P, Kasubi MJ, Haarr L, Bergstrom T, Liljeqvist J-A. 2007. Divergence and recombination of clinical herpes simplex virus type 2 isolates. J Virol 81:13158–13167.

15. Norberg P, Tyler S, Severini A, Whitley R, Liljeqvist J-A, Bergstrom T. 2011. A genome-wide comparative evolutionary analysis of herpes simplex virus type 1 and varicella zoster virus. PloS One 6:1–8.

16. Newman RM, Lamers SL, Weiner B, Ray SC, Colgrove RC, Diaz F, Jing L, Wang K, Saif S, Young S, Henn M, Laeyendecker O, Tobian AAR, Cohen JI, Koelle DM, Quinn TC, Knipe DM. 2015. Genome Sequencing and Analysis of Geographically Diverse Clinical Isolates of Herpes Simplex Virus 2. J Virol JVI.01303-15.

17. Johnston C, Magaret A, Roychoudhury P, Greninger AL, Reeves D, Schiffer J, Jerome KR, Sather C, Diem K, Lingappa JR, Celum C, Koelle DM, Wald A. 2017. Dual-strain genital herpes simplex virus type 2 (HSV-2) infection in the US, Peru, and 8 countries in sub-Saharan Africa: A nested cross-sectional viral genotyping study. PLOS Med 14:e1002475.

18. Larkin MA, Blackshields G, Brown NP, Chenna R, McGettigan PA, McWilliam H, Valentin F, Wallace IM, Wilm A, Lopez R, Thompson JD, Gibson TJ, Higgins DG. 2007. Clustal W and Clustal X version 2.0. Bioinforma Appl Note 23:2947–2948.

19. Kolb AW, Larsen IV, Cuellar JA, Brandt CR. 2015. Genomic, Phylogenetic, and Recombinational Characterization of Herpes Simplex Virus 2 Strains. J Virol 89:6427–6434.

20. Johnston C, Magaret A, Roychoudhury P, Greninger AL, Cheng A, Diem K, Fitzgibbon MP, Huang M, Selke S, Lingappa JR, Celum C, Jerome KR, Wald A, Koelle DM. 2017. Highly conserved intragenic HSV-2 sequences: Results from next-generation sequencing of HSV-2 U L and U S regions from genital swabs collected from 3 continents. Virology 510:90–98.

21. Deschamps T, Kalamvoki M. 2017. Impaired STING Pathway in Human Osteosarcoma U2OS Cells Contributes to the Growth of ICP0-Null Mutant Herpes Simplex Virus. J Virol 91:e00006-17.

22. Davison AJ. 2012. Evolution of sexually transmitted and sexually transmissible human herpesviruses. Ann N Y Acad Sci 1230:E37–E49.

23. Colgrove R, Diaz F, Newman R, Saif S, Shea T, Young S, Henn M, Knipe DM. 2014. Genomic sequences of a low passage herpes simplex virus 2 clinical isolate and its plaque-purified derivative strain. Virology 450–451:140–145.

24. Lai W, Chen CY, Morse SA, Htun Y, Fehler HG, Liu H, Ballard RC. 2003. Increasing relative prevalence of HSV-2 infection among men with genital ulcers from a mining community in South Africa. Sex Transm Infect 79:202–207.

25. Koelle DM, Norberg P, Fitzgibbon MP, Russell RM, Greninger AL, Huang M-L, Stensland L, Jing L, Magaret AS, Diem K, Selke S, Xie H, Celum C, Lingappa JR, Jerome KR, Wald A, Johnston C. 2017. Worldwide circulation of HSV-2 × HSV-1 recombinant strains. Sci Rep 7:44084.

26. Foster TP, Chouljenko VN, Kousoulas KG. 2008. Functional and physical interactions of the herpes simplex virus type 1 UL20 membrane protein with glycoprotein K. J Virol 82:6310–6323.

27. David AT, Saied A, Charles A, Subramanian R, Chouljenko VN, Kousoulas KG. 2012. A Herpes Simplex Virus 1 (McKrae) Mutant Lacking the Glycoprotein K Gene Is Unable To Infect via Neuronal Axons and Egress from Neuronal Cell Bodies. mBio 3.

28. David AT, Baghian A, Foster TP, Chouljenko VN, Kousoulas KG. 2008. The Herpes Simplex Virus Type 1 (HSV-1) Glycoprotein K(gK) is Essential for Viral Corneal Spread and Neuroinvasiveness. Curr Eye Res 33:455–467.

29. Johnson DC, Frame MC, Ligas MW, Cross AM, Stow ND. 1988. Herpes simplex virus immunoglobulin G Fc receptor activity depends on a complex of two viral glycoproteins, gE and gI. J Virol 62:1347–1354.

30. Dingwell KS, Brunetti CR, Hendricks RL, Tang Q, Tang M, Rainbow AJ, Johnson DC. 1994. Herpes simplex virus glycoproteins E and I facilitate cell-to-cell spread in vivo and across junctions of cultured cells. J Virol 68:834–845.

31. Dingwell KS, Doering LC, Johnson DC. 1995. Glycoproteins E and I facilitate neuron-to-neuron spread of herpes simplex virus. J Virol 69:7087–7098.

32. Lu X, Huang C, Zhang Y, Lin Y, Wang X, Li Q, Liu S, Tang J, Zhou L. 2017. The Us2 Gene Product of Herpes Simplex Virus 2 modulates NF-κB activation by targeting TAK1. Sci Rep 7:8396.

33. Weber PC, Levine M, Glorioso JC. 1987. Rapid identification of nonessential genes of herpes simplex virus type 1 by Tn5 mutagenesis. Science 236:576–579.

34. Meignier B, Longnecker R, Mavromara-Nazos P, Sears AE, Roizman B. 1988. Virulence of and establishment of latency by genetically engineered deletion mutants of herpes simplex virus 1. Virology 162:251–254.

35. Viejo-Borbolla A, Martinez-Martín N, Nel HJ, Rueda P, Martín R, Blanco S, Arenzana-Seisdedos F, Thelen M, Fallon PG, Alcamí A. 2012. Enhancement of chemokine function as an immunomodulatory strategy employed by human herpesviruses. PLoS Pathog 8:e1002497.

36. Cabrera JR, Viejo-Borbolla A, Martinez-Martín N, Blanco S, Wandosell F, Alcamí A. 2015. Secreted herpes simplex virus-2 glycoprotein G modifies NGF-TrkA signaling to attract free nerve endings to the site of infection. PLoS Pathog 11:e1004571.

37. Lymberopoulos MH, Pearson A. 2007. Involvement of UL24 in herpes-simplex-virus-1-induced dispersal of nucleolin. Virology 363:397–409.

38. Jacobson JG, Martin SL, Coen DM. 1989. A conserved open reading frame that overlaps the herpes simplex virus thymidine kinase gene is important for viral growth in cell culture. J Virol 63:1839–1843.

39. Rochette P-A, Bourget A, Sanabria-Solano C, Lahmidi S, Lavallée GO, Pearson A. 2015. Mutation of UL24 impedes the dissemination of acute herpes simplex virus 1 infection from the cornea to neurons of trigeminal ganglia. J Gen Virol 96:2794–2805.

40. Leiva-Torres GA, Rochette P-A, Pearson A. 2010. Differential importance of highly conserved residues in UL24 for herpes simplex virus 1 replication in vivo and reactivation. J Gen Virol 91:1109–1116.

41. Jacobson JG, Chen SH, Cook WJ, Kramer MF, Coen DM. 1998. Importance of the herpes simplex virus UL24 gene for productive ganglionic infection in mice. Virology 242:161–169.

42. Foster TP, Alvarez X, Kousoulas KG. 2003. Plasma membrane topology of syncytial domains of herpes simplex virus type 1 glycoprotein K (gK): the UL20 protein enables cell surface localization of gK but not gK-mediated cell-to-cell fusion. J Virol 77:499–510.

43. Foster TP, Melancon JM, Baines JD, Kousoulas KG. 2004. The herpes simplex virus type 1 UL20 protein modulates membrane fusion events during cytoplasmic virion morphogenesis and virus-induced cell fusion. J Virol 78:5347–5357.

44. Foster TP, Melancon JM, Olivier TL, Kousoulas KG. 2004. Herpes simplex virus type 1 glycoprotein K and the UL20 protein are interdependent for intracellular trafficking and trans-Golgi network localization. J Virol 78:13262–13277.

45. Liu J, Lewin AS, Tuli SS, Ghivizzani SC, Schultz GS, Bloom DC. 2008. Reduction in severity of a herpes simplex virus type 1 murine infection by treatment with a ribozyme targeting the UL20 gene RNA. J Virol 82:7467–7474.